A modular CRISPR screen identifies individual and combination pathways contributing to HIV-1 latency

Emily Hsieh[1], Derek H Janssens[2], Patrick J Paddison[3], Edward P Browne[4], Steve Henikoff[2,5], Molly OhAinle[3,6], Michael Emerman[2,3*]

[1]Molecular and Cellular Biology Graduate Program, University of Washington, Seattle, WA, USA
[2]Division of Basic Sciences, Fred Hutchinson Cancer Center, Seattle, WA, USA
[3]Division of Human Biology, Fred Hutchinson Cancer Center, Seattle, WA, USA
[4]Division of Infectious Diseases, Department of Medicine, University of North Carolina at Chapel Hill, Chapel Hill, NC, USA
[5]Howard Hughes Medical Institute, Chevy Chase, MD, USA
[6]current address: Division of Immunology and Molecular Medicine, Department of Molecular and Cell Biology, University of California, Berkeley, CA, USA

*Corresponding author: Michael Emerman, memerman@fredhutch.org

Abstract

Transcriptional silencing of latent HIV-1 proviruses entails complex and overlapping mechanisms and are a major barrier to *in vivo* elimination of HIV-1. We developed a new latency CRISPR screening strategy, called Latency HIV-CRISPR, which uses the packaging of guideRNA-encoding lentiviral vector genomes into the supernatant of budding virions as a direct readout of factors involved in the maintenance of HIV-1 latency. We developed a custom guideRNA library targeting epigenetic regulatory genes and paired the screen with and without a latency reversal agent – AZD5582, an activator of the non-canonical NFκB pathway – to examine a combination of mechanisms controlling HIV-1 latency. A component of the Nucleosome Acetyltransferase of H4 histone acetylation (NuA4 HAT) complex, ING3, acts in concert with AZD5582 to activate proviruses in J-Lat cell lines and in a primary CD4+ T cell model of HIV-1 latency. We found that the knockout of *ING3* reduces acetylation of the H4 histone tail and BRD4 occupancy on the HIV-1 LTR, and the combination of *ING3* knockout with the activation of non-canonical NFκB via AZD5582 act together to dramatically increase initiation and elongation of RNA Polymerase II on the HIV-1 provirus in a manner that is nearly unique among all cellular promoters.

42 **Introduction**
43
44 Effective antiretroviral therapy (ART) can drive HIV-1 viral loads to undetectable
45 levels [1]. However, ART does not eliminate the virus from people living with HIV-1.
46 Upon interruption of ART, there is a rapid rebound of virus replication from a long-lived
47 latent reservoir primarily found in memory CD4+ T cells among other cell types [2]. This
48 latent reservoir of replication-competent HIV-1 proviruses is a significant obstacle to the
49 complete clearance of HIV-1 [3], and purging or managing this latent reservoir is
50 essential to achieve a functional cure.
51 The latent HIV-1 reservoir is often transcriptionally silent but can produce
52 infectious virus upon T-cell activation [4]. The transcriptional silencing of the provirus in
53 HIV-1 latency is dependent on integration site [5, 6] and a breadth of host factors that
54 limit transcriptional initiation and elongation of the HIV-1 proviral genome [7]. Small
55 molecule inhibitors or activators, known as latency reversal agents (LRAs), have been
56 shown to activate HIV-1 viral transcription in cell line models of HIV-1 latency [8] and in
57 primary cell cultures derived from people living with HIV-1 [9, 10]. AZD5582 is a second
58 mitochondria-derived activator of caspases (SMAC) mimetic that is an example of an
59 LRA that provides some specificity for latency reversal by activating the non-canonical
60 NFκB pathway [11]. Many LRAs have shown success at reactivating latent HIV-1 in
61 HIV-1 latency models, but even the most well-established LRAs have modest or no
62 effect in clinical trials on their own [12]. This highlights the complexity of mechanisms
63 involved in maintaining the HIV-1 latent state, and the need to identify novel epigenetic
64 factors and transcriptional mechanisms controlling HIV-1 latency.

65

66 Studies on the functional role of host epigenetic regulation of HIV-1 transcription
67 (reviewed in [7, 13, 14]) has resulted in the identification of some specific host
68 epigenetic regulatory genes that are involved in maintaining HIV-1 latency. For
69 example, KAT5 of the Nucleosome Acetyltransferase of H4 histone acetylation (NuA4
70 HAT) complex deposits a uniquely high profile of acetylated lysine residues on the H4
71 histone tail (H4Ac) found at the HIV-1 provirus LTR [9]. This results in the recruitment of
72 the long isoform of the *Bromodomain Containing 4* (*BRD4*) gene [9, 15, 16].
73 Additionally, the long BRD4 isoform serves as a competitor for positive transcription
74 elongation factor b (P-TEFb) binding to the HIV-1 transactivator, Tat [16]. *BRD4* also
75 encodes a short isoform that recruits the repressive BAF complex to the HIV-1 provirus
76 [17]. Another set of genes implicated in HIV-1 latency encode components of the
77 Polycomb Repressive Complex 2 (PRC2) which catalyzes the methylation of histone H3
78 Lysine 27 to maintain transcriptional repression of genes, including throughout
79 development [10, 18, 19].
80 The use of genetic screens has been effective in revealing pathways involved in
81 HIV-1 latency in a single-gene manner [10, 20-27]. Here, we sought to create a novel
82 CRISPR-based screening platform with the capacity to allow for rapid, parallel
83 assessment of multiple pathways that contribute to the maintenance of HIV-1 latency
84 both with and without the presence of additional LRAs. We reasoned that by combining
85 LRAs of one mechanism with a CRISPR screen that targets a different mechanism, we
86 could uncover latency reversal pathways with increased potency and specificity for the

87 HIV-1 LTR. We established a novel HIV-based latency CRISPR screening strategy that
88 uses J-Lat cells [28, 29] in combination with our recently developed HIV-CRISPR
89 screening methodology [30] to use reactivation of the latent provirus as the reporter for
90 the screen. To identify epigenetic pathways that act with and without LRAs to activate
91 latent proviruses, we generated a custom CRISPR library targeting epigenetic
92 regulatory genes and performed the screen in the absence and presence of a low dose
93 of AZD5582. In the absence of AZD5582, we found *CUL3*, a scaffold for an E3 ubiquitin
94 ligase, as a novel HIV-1 latency maintenance and establishment factor in both J-Lat
95 cells and a primary CD4+ T cell model of HIV-1 latency. Moreover, we identified the
96 NuA4 HAT complex to be of importance to HIV-1 latency, specifically two complex
97 subunit members – ACTL6A and ING3. In particular, *Inhibitor of Growth Family Member*
98 *(ING3)* knockout combined with AZD5582 treatment resulted in enhanced viral
99 reactivation in the J-Lat cells and a primary CD4+ T cell model of HIV-1 latency. By
100 using automated CUT&Tag to investigate genome-wide chromatin occupancy [31], we
101 found that *ING3* knockout alone and in combination with AZD5582 treatment causes
102 H4Ac and BRD4 levels to be reduced at the HIV-1 LTR. However, only in the presence
103 of AZD5582 in the *ING3* knockout cells, do we see a substantial increase in RNA
104 Polymerase II Serine 5 phosphorylation (RNA-Pol2-S5p) occupancy at the LTR and this
105 dramatic increase is nearly unique among all promoters in the human genome.
106 Simultaneously, the combination of *ING3* knockout and AZD5582 treatment results in
107 increases in RNA-Pol2-S5p and RNA-Pol2-S2p within the body of the provirus, which
108 indicates increased transcription initiation and elongation and correlates with the

109 increases of viral reactivation. Our novel HIV-CRISPR screening approach provides an
110 avenue to explore factors that act in combination to promote HIV-1 latency.
111
112 **Results**
113
114 Latency HIV-CRISPR identifies novel epigenetic factors involved in maintaining HIV-1
115 latency
116 Our aim was to establish a high throughput CRISPR-Cas9 knockout strategy
117 using the biology of HIV-1 packaging and budding to facilitate a screen for investigating
118 the complexities of epigenetic regulation of HIV-1 latency. This approach uses a
119 previously described HIV-CRISPR vector [30] which is a lentiviral based vector with two
120 intact LTRs, a packaging signal, Cas9, and a library of single guide RNAs (sgRNAs).
121 The unique feature of the HIV-CRISPR vector is that in the presence of replication-
122 competent HIV-1, the genome of the HIV-CRISPR vector is transcribed into RNA and
123 packaged *in trans* into HIV-1 virions. We reasoned that in J-Lat cells, an *in vitro* T-
124 lymphocyte HIV-1 latency model which harbors a near full-length HIV-1 provirus, any
125 sgRNAs encoded in HIV-CRISPR genomes that target candidate HIV-1 latency genes
126 will be packaged into the reactivated virus particle, secreted, and enriched in the viral
127 supernatant (**Figure 1A**). Consequently, the RNA of the viral supernatant from the HIV-
128 CRISPR latency screen can undergo next-generation sequencing to determine sgRNAs
129 that are enriched in the viral particles and thereby identify candidate genes involved in
130 HIV-1 latency maintenance. This results in a direct readout for the gene knockout which
131 incorporates functional, reactivation activity.

132 To specifically investigate host epigenetic regulators involved in the maintenance
133 of HIV-1 latency, we generated a custom human epigenome specific sgRNA CRISPR
134 library (HuEpi). This library contains sgRNAs targeting epigenome factors such as
135 histones, histone binders (e.g., histone readers and chaperones), histone modifiers
136 (e.g., histone writers and erasers), and general chromatin associated factors (e.g., RNA
137 and DNA modifiers) (**Figure 1B, C**). Most of the genes targeted in this library are
138 derived from the EpiFactor database [32]. To this set we also added histones and other
139 hand-selected gene regulatory complexes. The total library contains 5,309 sgRNAs
140 targeting 841 genes (6 sgRNAs per gene with a few exceptions) and 252 non-targeting
141 controls (NTCs) [33] (**Supplemental Table 1**). The small size of the library improves the
142 likelihood of high coverage of all the sgRNAs throughout the CRISPR screening
143 process relative to a whole-genome screen.

144 The sgRNA sequences from the HuEpi library were cloned in bulk into the HIV-
145 CRISPR vector and the lentiviral library was subsequently transduced into J-Lat cells at
146 a low MOI (MOI = 0.4) (**Figure 1D-1**). We transduced two independent J-Lat cell clones,
147 the J-Lat 10.6 [28] and J-Lat 5A8 [29] cells, which each have different proviral
148 integration sites and the latter of which responds to LRAs more similarly to primary
149 CD4+ T cell HIV-1 latency models compared to other cell-line models [34]. Transduced
150 cells were then subjected to 10-14 days of puromycin selection after which the cells and
151 viral supernatant were harvested and processed by next-generation sequencing of the
152 sgRNAs to identify the candidate HIV-latency genes (**Figure 1D-3**). Genomic DNA was
153 extracted from the cell pellet to determine the baseline representation of each sgRNA in

154 the transduced sgRNA library. Viral RNA was extracted from the concentrated viral
155 supernatant to identify the sgRNA population that facilitated latent HIV-1 provirus
156 transcription reactivation (**Figure 1D-4**). Using the MAGeCK pipeline [35], we identified
157 candidate HIV-1 latency maintenance factors by selecting genes in which the sgRNA
158 counts of the viral RNA were enriched compared to the sgRNA counts in the genomic
159 DNA. Genes with an increased sgRNA count in the viral RNA, which equates to an
160 increase in the fold change, are predicted to play a role in maintaining HIV-1 latency.

161 Overall, the Latency HIV-CRISPR screen results for both J-Lat 10.6 and J-Lat
162 5A8 cell lines demonstrated a significant enrichment in specific sgRNAs compared to
163 the NTCs. We compared the distribution of the log fold change (LFC) of NTCs against
164 the gene targeting sgRNAs. While the LFC of most gene targeting sgRNAs clustered
165 around the median LFC of the NTCs, we observed that a subset of the gene targeting
166 sgRNAs were significantly enriched compared to the NTC population. These sgRNAs
167 are the sgRNAs of interest that target potential HIV-1 latency maintenance factor genes
168 (**Figure 2A**).

169 To determine top candidate genes from the Latency HIV-CRISPR screen, we
170 ranked the genes by MAGeCK gene score. For both J-Lat cell lines, we observe that
171 there are many genes that are significantly enriched compared to the NTCs. We
172 identified eight previously unreported epigenetic HIV-1 latency maintenance genes,
173 defined by a false discovery rate (FDR) less than 10% in both J-Lat 10.6 and J-Lat 5A8
174 cell lines, as our top hits and they are labelled in the figure (**Figure 3A**). BRD4 and
175 KAT5 are two host factors previously reported to silence HIV-1 transcription ([16, 17, 36]

176 and [9], respectively), and in our screen, the sgRNAs targeting *BRD4* and *KAT5* are
177 significantly enriched compared to the sgRNAs targeting NTCs in both J-Lat cell lines
178 (**Figure 2B; Supplemental Table 2**). In addition to individual genes, the Latency HIV-
179 CRISPR screen also identified genes encoding subunits of protein complexes important
180 to HIV-1 latency. PRC2 has also been previously reported to silence HIV-1 transcription
181 [8, 10] and members of the complex including *EZH2*, the catalytic component, and
182 *SUZ12* and *EED* showed a trend of enrichment in our screen (**Figure 2B;**
183 **Supplemental Table 2**). Thus, our Latency HIV-CRISPR screen system identifies bona
184 fide HIV-1 latency maintenance factors.
185
186 <u>The Latency HIV-CRISPR screen identifies multiple members of the NuA4 complex and</u>
187 <u>CUL3</u>
188 To identify the top candidate HIV-1 latency genes, we integrated the guideRNA
189 data to a gene level using MAGeCK analysis [35] (**Figure 3A; Supplemental Table 3**).
190 As we were primarily interested in hits that are independent of integration site, we
191 considered the top gene hits as those that that have an FDR < 10% and also are shared
192 between both J-Lat 10.6 and J-Lat 5A8 cell lines (**Figure 3B**, middle of Venn diagram).
193 We observed that multiple members of the Nucleosome Acetyltransferase of H4 (NuA4)
194 complex scored highly in the screen (**Figure 3A**). The NuA4 complex is highly
195 conserved in eukaryotes [37] and acetylates histone H4 [38] and has been implicated in
196 many genomic processes including DNA damage repair and transcription [39]. Many
197 proteins that are part of the NuA4 complex also overlap with the SNF2-Related CBP

198 Activator Protein (SRCAP) complex which exchanges the H2A of the canonical
199 nucleosome with the H2A.Z variant [40-42]. A gene ontology (GO) enrichment analysis
200 [43] of the top gene hits (FDR <10% for each J-Lat cell line) demonstrated that the
201 SRCAP-associated chromatin remodeling complex is highly enriched in both J-Lat cell
202 lines (**Figure 3C**). Based on the MAGeCK gene scores, six of the seven genes (*BRD8*,
203 *DMAP1*, *RUVBL1*, *RUVBL2*, *ACTL6A*, *VPS72*, and *YEATS4*) that encode proteins
204 overlapping between the NuA4 HAT and SRCAP complexes scored higher than the
205 median MAGeCK score for the NTCs (**Figure 3D**). The only exception is *RUVBL1* in the
206 J-Lat 10.6 screen, which scored below the NTC median MAGeCK score (RUVBL1 =
207 0.318 vs NTC median = 0.518). Additionally, most genes unique to each complex also
208 had MAGeCK scores above the NTC median in both cell lines. Genes unique to the
209 NuA4 HAT complex included *TRRAP*, *EP400*, *EPC2*, *KAT5*, *ING3*, *MORF4L1*,
210 *MORF4L2*, *MEAF6*, and *MBTD1* and genes unique to the SRCAP complex included
211 *SRCAP* and *ZNHIT1* (**Figure 3D**). This analysis suggests that the Latency HIV-CRISPR
212 screen strategy can extend beyond identification of single genes of interest to groups of
213 genes encoding complexes of relevance, which can further shed light on the
214 mechanisms involved in maintaining HIV-1 latency.

215 To validate the top screen hits, we generated four individual J-Lat 10.6 and 5A8
216 knockout cell lines for each gene (two sgRNAs per gene). As positive controls, we used
217 two sgRNAs targeting *NFκBIA*, an inhibitor for NFκB, and a gene that was not included
218 in the HuEpi library. Upon knockout of *NFκBIA* in the J-Lat cells, we expect an increase
219 in HIV-1 transcriptional activity, which leads to virus production. As negative controls,

220 we used two NTC sgRNAs that do not target human loci. To assess latency reversal in
221 the J-Lat cells, we measured HIV-1 reverse transcriptase activity in the supernatant,
222 which is a readout after the viral transcription, translation, and budding steps have
223 occurred. Because the transduced cells were assayed as a pool of gene knockouts, we
224 simultaneously measured CRISPR editing efficiency in bulk using the program
225 Inference of CRISPR Edits (ICE) [44]. The knockout efficiency for the heterogenous cell
226 lines we generated varied between 32% to 83% (**Figure 4A**). A recent study
227 demonstrated that a median knockout of 35% was less efficient, but still had a
228 meaningful effect [45].

229 Compared to the cell lines transduced with NTC sgRNAs, we found that
230 individually knocking out all eight novel candidate gene hits resulted in significant
231 latency reversal in at least one of the J-Lat cell lines we tested (**Figure 4A**). In fact,
232 some of the reverse transcriptase measurements from the gene knockout cell lines are
233 comparable to the positive control knockout of *NFκBIA*. In addition, we confirmed that
234 knockout of a top scoring gene hit in our screen, *KAT5*, a previously reported HIV-1
235 latency maintenance factor [9], results in viral reactivation in both J-Lat cell lines (**Figure**
236 **4A**). Moreover, genes encoding protein components of the NuA4 HAT and SRCAP
237 complexes described above, *ACTL6A*, *DMAP1*, *VPS72*, and *YEATS4* also all validated
238 as latency maintenance factors in J-Lat cells (**Figure 4A**). *ACTL6A* knockout, in
239 particular, results in a high level of HIV-1 reactivation, which may be a result of *ACTL6A*
240 encoding a protein that is a subunit of both NuA4 HAT and SRCAP complexes (**Figure**
241 **3D**). Other genes validated in this functional investigation include *DMAP1* which

242 encodes a protein that forms a complex with DNMT1 to mediate transcriptional
243 repression [46] and has been described to play a role in HIV-1 latency in some studies
244 [14] and *TAF5* which functions in scaffold formation and is a critical subunit of the
245 general transcription factor TFIID.

246 As *CUL3* was the top gene hit in our Latency HIV-CRISPR screen in both J-Lat
247 10.6 and J-Lat 5A8 cell lines and validated as a latency maintenance factor in J-Lat
248 cells, we further characterized *CUL3* in the context of a primary CD4+ T cell HIV-1
249 latency model system. CUL3 is part of the cullin family and serves as the scaffold for
250 Cullin-RING E3 ligase complexes, which ubiquitinate proteins [47]. For our primary cell
251 HIV-1 latency model system, we used a dual HIV-1 reporter virus (pNL4-3-Δ6-dreGFP-
252 CD90) that is derived from previously established systems [48, 49]. Here, the reporter
253 virus has been modified to encode a destabilized eGFP gene and a mouse Thy1.2
254 (CD90.2) gene, which are separated by an IRES and both reporters are under control of
255 the HIV-1 LTR [50]. As the mouse Thy1.2 reporter has a long half-life and is slow to turn
256 over, it serves as a marker to determine the cells that have been infected by the
257 reporter virus (Thy1.2+). Amongst the infected cells (Thy1.2+), the eGFP reporter,
258 which has a short half-life, serves as a marker to determine the cells that are actively
259 transcribing or actively infected (Thy1.2+, GFP+) versus minimally transcribing or
260 latently infected (Thy1.2+, GFP-). We knocked out *CUL3* in the primary CD4+ T cell
261 HIV-1 latency model using Cas9-gRNA ribonucleoproteins (RNPs) including 3 different
262 sgRNAs. As a negative control, the *AAVS1* gene is targeted for knockout, which is in a

263 “safe harbor” locus in which disruption of this gene does not have adverse effects on the
264 cell [51].

265 We expected that if CUL3 plays a role in HIV-1 latency establishment, there will
266 be a higher reactivated population in the *CUL3* knockout cells compared to the negative
267 control (*AAVS1*) knockout cells. We acquired CD4+ T cells from four healthy donors and
268 infected the cells with the dual reporter virus. Indeed, upon performing the described
269 CRISPR/Cas9-mediated knockout and measuring the functional output of the reporter
270 virus, we observed that *CUL3* knockout in all four donors resulted in significant HIV-1
271 reactivation and subsequent decrease in the latent population compared to *AAVS1*
272 knockout (**Figure 4C; Supplemental Figure 4A**). This suggests that post-translational
273 ubiquitin modification by CUL3 of a substrate may facilitate the establishment and
274 maintenance of HIV-1 latency. Our data is consistent with previous work as CUL3 has
275 been demonstrated to negatively regulate HIV-1 transcription during productive infection
276 through the NFκB pathway [52]. Moreover, these data demonstrate that the Latency
277 HIV-CRISPR screening strategy is effective in identifying novel epigenetic HIV-1 latency
278 maintenance genes that have been validated in multiple systems.

279

280 <u>An LRA Latency HIV-CRISPR screen reveals regulatory changes that act in</u>
281 <u>combination during reactivation of HIV-1 latency</u>

282 A critical extension of this HIV-CRISPR latency screen methodology is the ability
283 to examine other transcriptional mechanisms in conjunction with epigenetic regulation
284 factors. Thus, to address HIV-1 latency as a state of multiple, parallel mechanisms, we

285 modified the screen by treating the pool of human epigenome knockout cells with a low-
286 activating dose of LRA. The goal was to identify instances of combinations between the
287 gene knockout and LRA resulting in a significant increase in viral reactivation (i.e. a top
288 hit in the screen). As a proof of principle, we used the recently identified LRA, AZD5582,
289 which is a SMAC mimetic and non-canonical NFκB activator [11]. We first determined
290 10 nM AZD5582 as the low-activating dose of LRA to use by performing an HIV-1 viral
291 reactivation dose curve using both J-Lat cell lines (**Supplemental Figure 5A**). The
292 same HuEpi knockout pool of cells used in the Latency HIV-CRISPR screen described
293 in **Figure 3** were in parallel treated for 24 hours with 10 nM of AZD5582 (**Figure 1D-4**)
294 to identify epigenetic regulatory genes that upon knockout, combine with the
295 transcriptional initiation pathway targeted by AZD5582, to result in a significant increase
296 in viral reactivation.

297 The most prominent hit of the AZD5582 LRA Latency HIV-CRISPR screen in
298 both J-Lat cell lines was *Inhibitor of Growth Family Member 3* (*ING3*), a novel HIV-1
299 latency factor (**Figure 5A; Supplemental Table 4, 5**). To confirm that *ING3* was a top
300 gene hit unique to the LRA condition, we compared the LRA Latency HIV-CRISPR
301 screen results to the Latency HIV-CRISPR screen results in the absence of LRA.
302 Overall, many gene hits overlapped between the Latency HIV-CRISPR screen in the
303 presence and absence of AZD5582 (**Figure 5B**). For example, the previously identified
304 *KAT5* gene and genes that we validated in **Figure 4** including *DNMT1*, *YEATS4*, and
305 *ACTL6A* were still amongst the top gene hits, which suggests that these genes broadly
306 play a role in HIV-1 latency maintenance regardless of activation of the non-canonical

307 NFκB pathway. We verified that *ING3* was the top gene hit unique to the screen in the
308 presence of AZD5582 and sought to perform additional validation for this gene. We also
309 observed that *CUL3*, the top hit unique to the screen in the absence of AZD5582, was
310 relatively depleted in the screen conducted in the presence of AZD5582 (**Figure 5B**).
311 This suggests a potential overlap between AZD5582 non-canonical NFκB function and
312 *CUL3* function in the context of HIV-1 latency reversal.

313 To validate *ING3*, the top hit enriched in the AZD5582 LRA Latency HIV-CRISPR
314 arm of the screen, we generated *ING3* knockout cell lines in both J-Lat 10.6 and 5A8
315 cells. Simultaneously, cell lines transduced with the NTC sgRNAs were generated as a
316 negative control. The pools of knockout cells were treated with or without a low
317 reactivating dose (10 nM) of AZD5582 for 24 hours and then viral reactivation was
318 measured by HIV-1 reverse transcriptase activity. Based on screen results, we
319 hypothesized that knockout of *ING3* alone would result in some level of viral reactivation
320 compared to the transduction of NTC sgRNAs, but upon treatment with a low
321 reactivating dose of AZD5582, viral reactivation would become even more pronounced.
322 Consistent with our hypothesis, we observed that in both J-Lat cell lines, low
323 reactivating dose AZD5582 treatment of the cell lines transduced with the NTC sgRNAs
324 results in minimal viral reactivation, but treatment of the *ING3* knockout cell lines results
325 in significant, increased viral reactivation (**Figure 6A**). These results suggest a
326 mechanistic interplay between *ING3* inhibition and AZD5582 treatment during the
327 reactivation of HIV-1 transcription. Moreover, we observed a similar trend in the primary
328 CD4+ T cell HIV-1 latency model described previously. In one healthy donor sample of

329 CD4+ T cells in which the latency model was established, we performed three
330 independent *AAVS1* and *ING3* knockouts, followed by 1 μM AZD5582 treatment, and
331 observed significant viral reactivation in the combination condition of *ING3* knockout and
332 AZD5582 treatment (**Figure 6B, C**). We observed similar results in a total of two healthy
333 donor samples of CD4+ T cells (**Supplemental Figure 6A**). This enhancement of viral
334 reactivation in two latency models suggests that there may be interplay between the
335 function of *ING3* and the non-canonical NFκB pathway, which is targeted by AZD5582,
336 both in cell lines and in primary CD4+ T cells.

337 As AZD5582 activates the non-canonical NFκB pathway, it is possible that *ING3*
338 knockout could either enhance this activity or act through an independent pathway in
339 the context of HIV-1 viral reactivation. To distinguish between these two possibilities, we
340 measured the protein levels of NFκB2 products which includes p100, the cytoplasmic
341 NFκB2 protein, and p52, the cleaved and active subunit that translocates to the
342 nucleus. As expected, activation of the non-canonical NFκB upon AZD5582 treatment
343 results in an increase in the cleaved p52 product and a decrease in the p100 product in
344 the control (NTC) cells (**Figure 6D**). We find that p52 levels are similar in the control
345 and *ING3* knockout J-Lat cell lines (**Figure 6D**) suggesting that another pathway
346 besides the non-canonical NFκB is the main driver resulting in HIV-1 reactivation.
347 Altogether the LRA Latency HIV-CRISPR screen demonstrates the powerful potential
348 for examining multiple mechanisms simultaneously to gain a more comprehensive
349 understanding of the mechanisms underpinning HIV-1 latency and to further improve
350 existing LRAs.

351

352 ING3 knockout in combination with AZD5582 treatment decreases pan-H4Ac and BRD4
353 levels and increases RNA-Pol2-S5p at the HIV-1 LTR

354 To better understand how AZD5582 treatment and *ING3* knockout act in
355 combination to promote reactivation of latent HIV-1 proviruses, we examined the
356 chromatin-related changes to the HIV-1 provirus by performing automated CUT&Tag
357 [31]. Specifically, we performed genome-wide profiling of the J-Lat 10.6 cell line under
358 four different conditions: (i) Transduction of NTC sgRNA with a treatment of DMSO
359 (NTC + DMSO), the negative control (ii) Transduction of NTC sgRNA with a treatment of
360 10 nM AZD5582 (NTC + AZD5582) (iii) *ING3* knockout with a treatment of DMSO (ING3
361 KO + DMSO) (iv) *ING3* knockout with a treatment of 10 nM AZD5582 (ING3 KO +
362 AZD5582).

363 ING3 is a known member of the NuA4 HAT complex, which functions to acetylate
364 the histone H4 tail [53]. BRD4 interacts with acetylated H4 [9] and both isoforms of
365 BRD4 are known to negatively regulate HIV-1 transcription [16, 17]. To examine
366 whether the reduction in *ING3* promotes activation of HIV-1 by modulating histone H4
367 acetylation and BRD4 occupancy on the HIV-1 LTR, we performed automated
368 CUT&Tag using antibodies that recognized acetylated histone H4 (pan-H4Ac), BRD4,
369 or a non-specific IgG negative control. As quality control, we determined the signal
370 levels of pan-H4Ac and BRD4 from the CUT&Tag data and confirmed the replicates of
371 each antibody were most highly correlated amongst each individual antibody
372 (**Supplemental Figure 7A**). We first examined pan-H4Ac marks at and around the HIV-

373 1 provirus. We observed no change in pan-H4Ac signal over the HIV-1 LTR upon 10 nM
374 AZD5582 treatment, but consistent with the known function of ING3, upon *ING3*
375 knockout, there was a significant decrease in pan-H4Ac signal at the HIV-1 LTR
376 (p=0.0061) (**Figure 7A, B**). Additionally, the combination of *ING3* knockout with
377 AZD5582 treatment, resulted in a significant decrease in pan-H4Ac signal at the HIV-1
378 LTR (p=0.0415). Notably, in the *ING3* knockout condition alone, we observed a
379 significant decrease in pan-H4Ac signal over both the U3 region of the HIV-1 LTR
380 (p=0.0070) as well as a significant decrease in the pan-H4Ac signal in the R and U5
381 region of the HIV-1 LTR (p=0.0126) containing the HIV-1 provirus transcription start site
382 (**Figure 7A, B**). When the *ING3* knockout is combined with AZD5582 treatment, there is
383 only a significant decrease in the R and U5 region of the HIV-1 LTR (p=0.0016). Thus,
384 *ING3* knockout appears to be the main driver of the change in pan-H4Ac levels on the
385 HIV-1 LTR in the presence and absence of AZD5582.

386 We hypothesized that the reduction in pan-H4Ac levels we observed on the HIV-
387 1 LTR in the *ING3* knockout condition would correlate with reduced recruitment of
388 BRD4. Indeed, as compared to NTC + DMSO, AZD5582 treatment alone did not affect
389 BRD4 levels over the HIV-1 LTR; however, BRD4 levels were significantly decreased
390 over the LTR both in the condition of *ING3* knockout alone and in combination with
391 AZD5582 treatment (p=0.0235, p=0.0349, respectively) (**Figure 7C, D**). In the absence
392 of AZD5582, the *ING3* knockout results in a significant decrease in the occupancy of
393 BRD4 only over the U3 region of the LTR (p=0.0219), while in the presence of AZD5582
394 combined with the *ING3* knockout, the decrease in BRD4 levels was only significant

395 over the R and U5 region of the HIV-1 LTR (p=0.0159) (**Figure 7C, D**). Thus, our pan-
396 H4Ac and BRD4 CUT&Tag results suggest that in the combination condition, the R and
397 U5 region of the HIV-1 LTR containing the HIV-1 transcription start site has a reduction
398 of inhibitory signals that likely contributes to the reactivation of the latent HIV-1 provirus.
399 Next, we examined the consequences of the decreased pan-H4Ac and BRD4
400 levels at the HIV-1 LTR by interrogating markers for transcription initiation and
401 elongation as mediated by the phosphorylation of RNA Polymerase II C-terminal
402 domain of Rpb1 (RNA-Pol2-S5p and RNA-Pol2-S2p, respectively) [54] at the HIV-1
403 LTR, body of the provirus ("provirus body"), and the region just downstream of the HIV-1
404 provirus integration site ("downstream"). Again, as quality control, we found the
405 CUT&Tag signal of the RNA-Pol2-S5p replicates were most highly correlated with one
406 another and were also correlated with the CUT&Tag signal of the RNA-Pol2-S2p
407 replicates (**Supplemental Figure 7B**). We find that there is a striking, significant
408 increase in RNA-Pol2-S5p signal at the HIV-1 LTR (p=4.2827E-5), provirus body
409 (p=8.943E-5), and downstream (p=2.03E-5) only in the condition where cells that are
410 knocked out for *ING3* and additionally treated with AZD5582. In contrast, for the RNA-
411 Pol2-S2p signal in cells with a combination of *ING3* knockout and AZD5582 treatment,
412 we observed a significant increase in the RNA-Pol2-S2p signal in the provirus body
413 (p=0.0458) and downstream region (p=3.89E-5), but not over the LTR (**Figure 7E, F**).
414 Interestingly, in the intermediate condition of only *ING3* knockout, the signal of RNA-
415 Pol2-S2p is significantly reduced at the HIV-1 LTR (p=0.00583) (**Figure 7G, H**). This
416 reduction in RNA-Pol2-S2p signal might be partially explained by the concomitant

417 reduction we see in pan-H4Ac signal at the HIV-1 LTR in the *ING3* knockout condition
418 alone. The striking increase in HIV-1 reverse transcriptase activity in the combination
419 condition is concordant with our CUT&Tag results and suggest that the knockout of
420 *ING3* combines with stimulation of the non-canonical NFκB pathway by AZD5582 to
421 promote a potent increase in the RNA-Pol2-S5p and RNA-Pol2-S2p on the HIV-1
422 proviral genome.

423 As we observed the most significant RNA-Pol2-S5p level changes in the
424 combined *ING3* knockout and AZD5582 treatment condition, we wondered whether
425 increased RNA-Pol2-S5p levels was occurring genome-wide or if this was specific to the
426 HIV-1 provirus. We compared the RNA-Pol2-S5p signal in the combined *ING3* knockout
427 cells treated with AZD5582 to the control (NTC + DMSO) condition. We found the RNA-
428 Pol2-S5p peaks over the HIV-1 LTR, provirus body, and downstream region were
429 amongst the peaks with the most significant increase in RNA-Pol2-S5p signal (**Figure**
430 **8A**). We then rank ordered all the RNA-Pol2-S5p peaks by Log_2-fold change and found
431 that out of the 2,547 total RNA-Pol2-S5p peaks, the top three peaks arranged from
432 highest to lowest fold change were the HIV-1 provirus body, the region downstream of
433 the HIV-1 integration site, and the HIV-1 LTR (**Figure 8B**). The two RNA-Pol2-S5p
434 peaks with a significant increase in signal and the next highest fold change cover
435 HCG27, a long non-coding RNA, and HIST2H4A – HIST2H4B, part of histone cluster 2
436 in the human genome. The RNA-Pol2-S5p peak with the strongest reduction in RNA-
437 Pol2-S5p signal in *ING3* knockout cells treated with AZD5582 covers PCGF3, a part of
438 the Polycomb group PRC1-like complex (**Figure 8B**). Overall, this suggests the

439 increase in transcription of the HIV-1 provirus caused by *ING3* knockout in combination
440 with AZD5582 treatment, as correlated to the RNA-Pol2-S5p mark, is highly specific and
441 nearly unique in the human genome. Thus, the CUT&Tag data reveal that *ING3*
442 knockout results in a reduction in H4Ac and BRD4 levels over the HIV-1 LTR and that
443 *ING3* knockout acts in combination with AZD5582 treatment to dramatically increase the
444 transcriptional initiation and transcription elongation of the HIV-1 provirus leading to
445 latency reversal.
446

447 **Discussion**

448 The hypothesis underlying this work is that modulating multiple overlapping
449 mechanisms that control HIV-1 LTR-driven transcription will increase the potency and
450 specificity of HIV-1 latency reactivation. That is, the goal is to find pathways that target
451 potent transcriptional activation of latent HIV-1 proviruses with minimal global effects.
452 We designed and validated a modular CRISPR screening approach which uses the
453 incorporation of HIV-CRISPR genomes encoding sgRNAs into budding virions as a
454 direct readout of activation of the latent provirus. The Latency HIV-CRISPR screen uses
455 a sgRNA library of epigenetic regulatory genes and is paired with and without an LRA,
456 AZD5582, to identify HIV-1 latency factors that act independently and in combination
457 with AZD5582. We identified *ING3* as a gene whose knockout resulted in an enhanced
458 increase of viral reactivation only in the presence of AZD5582. Using automated
459 CUT&Tag, we observed that this enhancement is associated with active transcription
460 marks as demonstrated by increased levels of RNA-Pol2-Ser5p and RNA-Pol2-Ser2p at

461 the HIV-1 genome and mechanistically may be dependent on a reduction in histone H4
462 acetylation and BRD4 occupancy over the HIV-1 LTR. We also identified CUL3 and
463 multiple members of the NuA4 HAT complex as important for HIV-1 latency
464 maintenance.
465
466 *Combinations of pathways with specificity for activating HIV-1 transcription*
467 We find that two independent mechanisms - *ING3* knockout and low-activating
468 dose of AZD5582 – which when combined, have unique, specific effects on the HIV-1
469 LTR and function together in order to efficiently activate HIV-1 transcription by
470 increasing the presence of initiated and elongating RNA-Pol2 at the LTR and within the
471 body of the HIV-1 provirus (**Figure 7**). Under these conditions used in our study, the
472 RNA-Pol2-S5p peaks with the highest fold change throughout the entire genome were
473 at the HIV-1 LTR and the provirus body (**Figure 8**). By CUT&Tag, RNA-Pol2-S5p
474 appears as the primary marker for HIV-1 transcription in the J-Lat 10.6 cell line and this
475 may be a result of P-TEFb, the major elongation factor for HIV-1 transcription, is a CTD
476 kinase that can phosphorylate Ser5 and Ser2 individually, but not simultaneously [55].
477 Our model suggests that a reduction in NuA4 acetylation and BRD4-dependent
478 occupancy specifically primes the HIV-1 LTR for enhanced transcription in response to
479 *ING3* knockout and activation of the non-canonical NFκB pathway.
480 Our observed effect of a reduction in histone acetylation and BRD4 recruitment
481 to the HIV-1 LTR that is concomitant with enhanced RNA-Pol2 initiation and elongation
482 suggests the HIV-1 provirus may be subject to unexpected transcriptional control. In

483 most mammalian transcriptional units driven by RNA-Pol2, NuA4 HAT is predominantly
484 localized to promoters of active genes, specifically around the transcription start sites
485 [56-58]. NuA4 HAT preferentially acetylates histone H4 [59] and this activity can impact
486 gene expression regulation to often result in activation of transcription. Moreover,
487 recruitment of other HAT complexes such as p300/CBP and P/CAF to the HIV-1 LTR
488 followed by subsequent acetylation is associated with stimulation, rather than silencing,
489 of HIV-1 transcription [60-66]. Additionally, using *in vitro* nucleosome-assembled
490 templates in a Tat-independent system, the NuA4 HAT activates HIV-1 transcription
491 [67]. Conversely, in the presence of Tat, the NuA4 HAT complex has been implicated in
492 silencing of HIV-1 transcription. For example, in both a primary CD4+ T cell model and
493 cells from ART-treated people living with HIV-1, the absence of KAT5, the catalytic
494 component of the NuA4 HAT complex, promotes activation of HIV-1 transcription as a
495 result of reduced H4 acetylation and BRD4 long isoform occupancy, and increased
496 levels of the Super Elongation Complex (SEC) members at the HIV-1 LTR [9]. Our
497 findings are consistent with this observation as our Latency HIV-CRISPR screen
498 identified multiple members of the NuA4 HAT complex, including KAT5, as top
499 candidates and all the candidates were validated as latency maintenance factors
500 through individual knockouts. In fact, our screen suggests that not only the catalytic
501 subunit, but the NuA4 HAT complex altogether regulates HIV-1 transcription negatively.
502 We observed a reduction in H4 acetylation across the entire HIV-1 LTR in
503 response to *ING3* knockout, but in the presence of AZD5582 we see the most
504 significant reduction of H4Ac signal and BRD4 occupancy at the R and U5 region which

505 includes the HIV-1 transcription start site. This observation suggests, the increase in
506 accessibility of the HIV-1 transcription start site when *ING3* knockout combined with
507 AZD5582 treatment likely promotes both transcription initiation and elongation,
508 culminating in the enhanced viral reactivation we observe in both J-Lat cells and primary
509 CD4+ T cell HIV-1 latency models. Additionally, the dosage of AZD5582 used was a
510 low-reactivating dose, suggesting that by inhibiting the NuA4 complex in parallel, it may
511 be possible to efficiently activate HIV-1 transcription while causing minimal disruptions
512 to a host system. HIV-1 is subject to complex transcriptional regulation, and these
513 results highlight the importance of simultaneously examining multiple mechanisms to
514 identify opportunities to specifically stimulate transcription of latent HIV-1 proviruses.
515 These results are similar in concept to a recent study that found that the combination of
516 AZD5582 and I-BET151 uniquely activated HIV-1 transcription in a Jurkat model of
517 latency [68].

518 In support of the hypothesis that these mechanisms are nearly unique to the HIV-
519 1 LTR, relatively few loci in the host genome showed a significant increase in RNA-
520 Pol2-S5p occupancy when *ING3* knockout is combined with a low-activating dose
521 treatment of AZD5582. One of these regions is downstream of the HIV-1 provirus
522 integration site in J-Lat 10.6 cells and part of the *SEC16A* gene (**Figure 8**). Activation of
523 human genes near or at the integrated provirus due to active transcription from an
524 integrated provirus is a likely scenario as HIV-1 preferentially integrates into highly
525 transcribed genes [69], and would be an unavoidable consequence of any reactivation
526 strategy used for eradicating the latent HIV-1 reservoir. In the combined condition of

527 *ING3* knockout and AZD5582 treatment, two other loci, a region of histone cluster 2
528 spanning HIST2H4A – HIST2H4B and a region overlapping with the long-noncoding
529 RNA, HCG27, also showed statistically significant, large fold changes in RNA-Pol2-S5p
530 levels, but these changes were not as prominent as those observed over the HIV-1
531 provirus (**Figure 8**). In addition, we observed the gene PCGF3 had significantly reduced
532 RNA-Pol2-S5p occupancy which could potentially to contribute to latency reversal as it
533 is part of the non-canonical Polycomb group RING finger 3/5-PRC1 complex with
534 silencing function [70] and is involved in the recruitment of PRC1 and PRC2 which have
535 been shown to contribute to HIV-1 proviral silencing [8, 10, 71].
536
537 *Comparison to other HIV latency screens*
538 Our Latency HIV-CRISPR screening strategy is a unique approach to identify
539 factors involved in HIV-1 latency. However, previous screens have also explored HIV-1
540 latency factors using gene knockout, knockdown, or silencing screening [10, 20-27].
541 Generally, these previous screens used whole genome sgRNA libraries which make
542 them unbiased for specific pathways, but this also limits the strength in statistical power
543 to determine gene hits. Nonetheless, these previous screens have uncovered an
544 exciting breadth of HIV-1 latency factors from the mTOR pathway [20] to proteasome
545 related genes [23, 25] to the non-canonical NFκB pathway [27]. As epigenetics plays an
546 important role in HIV-1 latency and it is still under investigation, we focused our Latency
547 HIV-CRISPR screen for epigenetic regulatory factors by using a small, custom designed
548 sgRNA library. Additionally, a smaller library can increase the dynamic range of a

549 screen [72]. Our screen also relies on the HIV-CRISPR vector [30] to perform a high-
550 throughput screen, which uses HIV-1 replication, rather than another reporter, as the
551 direct readout of the screen. The difference in readout from other screens including
552 screens with epigenetic hits [10, 22, 26] can result in different gene hits being
553 highlighted. Another challenge of studying mechanisms of HIV-1 latency is the
554 interaction of complex mechanisms in parallel and to address this using a CRISPR
555 screen approach, we combined the screen with a low-activating dose of LRA treatment.
556 By focusing our sgRNA library on epigenetic regulators and performing our screen with
557 and without AZD5582 treatment, we identified a unique combination of modifications
558 that synergize to stimulate HIV-1 transcriptional initiation and elongation. In the future,
559 by exploring the combination of additional LRAs with Latency HIV-CRISPR based
560 screens, we will improve the specificity and potency of novel LRAs and continue to work
561 towards a curative treatment strategy that eradicates the HIV-1 latent pool.
562

563 **Acknowledgements**

564 We thank Terry Hafer and Carley Gray for critical feedback of this manuscript, and
565 members of the Emerman lab for helpful suggestions and technical assistance. We
566 thank Warner Greene at Gladstone Institute of Virology and Immunology and University
567 of California, San Francisco, San Francisco, CA, USA for sharing the J-Lat 5A8 cells
568 and Darell Bigner at Duke University, Durham, NC, USA for sharing the H80 cells. We
569 thank Lucas Carter for assistance in assembly of the HuEpi library, Jackson Peterson
570 for discussions on the primary cell HIV-1 latency model, Daryl Humes and Hannah Itell

571 for discussions on primary cell protocols, and Matt Fitzgibbon and Pritha Chanana at
572 the FHCC for bioinformatics support. This work was supported by DP1 DA051110 (ME),
573 CARE 1UM1-A1-164567 (ME, EPB), University of Washington (UW) Viral Pathogenesis
574 training grant NIH T32 AI 083203 (EH), National Science Foundation Graduate
575 Research Fellowship DGE-1256082 and DGE-1762114 (EH), Hartwell Foundation
576 Postdoctoral Fellowship (DHJ), R01 DK119270-01 (PJP), NIDDK-U54DK106829 (PJP),
577 NIAID R01 AI143381 (EPB), NIDA R61 DA047023 (EPB), Howard Hughes Medical
578 Institute (SH), and R01 AI147877 (MO). Construction of the HuEpi library was
579 supported by a Fred Hutchinson Cancer Center Pathogen Associated Malignancy
580 Integrated Research Center award. This research was supported by the Genomics,
581 Bioinformatics, and Flow Cytometry Shared Resource, RRID:SCR_022606, of the Fred
582 Hutch/University of Washington Cancer Consortium (P30 CA015704).
583

584 **Figure Legends**
585
586 **Figure 1. The Latency HIV-CRISPR screen.**
587 **(A)** Schematic summarizing the Latency HIV-CRISPR screen in J-Lat cell lines showing
588 the latent, integrated provirus and the HIV-CRISPR vector which delivers Cas9 and a
589 sgRNA and produces a packageable genomic RNA. Red boxes represent the gene or
590 sgRNA targeting the gene of interest; gray boxes represent functional HIV-1 LTRs at
591 both sides of the vector and provirus; triangles represent internal promoters for sgRNA
592 and Cas9 transcription. **(B)** Categorical distribution of the genes targeted by the Human
593 Epigenome (HuEpi) sgRNA library. **(C)** Metascape Gene Ontology (GO) analysis [43] of
594 the genes targeted by the HuEpi sgRNA library. **(D)** Summary of workflow from the
595 generation of the pool of J-Lat HuEpi knockout cells to the sequencing and comparison
596 of the abundance of guideRNAs found in the viral RNA (vRNA) pool versus the genomic
597 DNA (gDNA) pool. GuideRNAs enriched in the viral supernatant RNA relative to the
598 genomic DNA represent the gene(s) that upon knockout result in latency reversal.
599
600 **Figure 2. GuideRNA level enrichment for known and novel genes of interest in the**
601 **Latency HIV-CRISPR screen.**
602 **(A)** GuideRNA enrichment (log_2 of fold change) in both J-Lat cell lines for the genes
603 targeted by the HuEpi sgRNA library compared to the Non-Targeting Control (NTC)
604 guides. For statistical analysis, the HuEpi gene sgRNAs are compared to the NTC
605 control. **(B)** GuideRNA level enrichment of known HIV-1 latency maintenance factors
606 BRD4, KAT5, and PRC2 complex members (EZH2, SUZ12, and EED) in the Latency
607 HIV-CRISPR screen. For statistical analysis, all conditions are compared to the NTC
608 control. Welch's t-test, p-value =<0.05 = *, =<0.05 = **, =<0.001 = ***.
609
610 **Figure 3. The Latency HIV-CRISPR screen in J-Lat 10.6 and J-Lat 5A8 cells**
611 **identifies a set of mutual, novel hits.**
612 **(A)** The $-log_{10}$ of the MAGeCK scores for each gene targeted by the HuEpi sgRNA
613 library (black circles and red triangles) and NTCs (gray squares) are calculated and
614 displayed. Gene names are labelled for hits that have a <10% false discovery rate
615 (FDR) in both J-Lat cell lines (center of Venn diagram in (B)); red triangles represent
616 members of the NuA4 HAT complex and SRCAP complex. NTCs are artificial NTC
617 genes designed by iterative binning of NTC sgRNA sequences (see Methods). Genes
618 are randomized on the x-axis, but the same order is used for both right and left panels.
619 The y-axis is the inverse log_{10} of the MAGeCK score. **(B)** Top hit genes (cut off of <10%
620 FDR) in common and unique to each J-Lat cell line are ordered by significance and
621 FDR with the top of the list having the highest significance and lowest FDR. **(C)**
622 Metascape GO analysis [43] of the gene hits with a <10% FDR in each J-Lat cell line.
623 (**D)** Analysis of the $-log_{10}$ of the MAGeCK scores of the genes overlapping and unique to
624 the NuA4 HAT and SRCAP complex compared to the NTCs. The higher the number,
625 the more statistically significant it is of a hit. Red font is for genes that score higher than
626 the average NTC score.
627

628 **Figure 4. Validation of top hits from Latency HIV-CRISPR screen.**
629 **(A)** Validation of the top 9 gene hits of the Latency HIV-CRISPR screen was performed
630 by individually knocking out each J-Lat cell line with two different guide RNAs and
631 measuring viral reactivation by quantifying HIV-1 reverse transcriptase activity of the
632 viral supernatant. *NFκBIA* knockout is a positive control. The reverse transcriptase
633 activity from released virions was normalized to basal activity from the NTC knockout.
634 For each for the knockout cell lines, ICE analysis was performed and the average
635 knockout is shown in pie charts. Multiple unpaired t-tests, p-value =<0.05 = *. **(B)** *CUL3*
636 knockout resulted in significant viral reactivation in a primary CD4+ T cell model of HIV-
637 1 latency using cells from four healthy donors. Viral reactivation was measured by flow
638 cytometry and normalized to the *AAVS1* knockout cells. Paired t-test, p-value =<0.05 =
639 *, =<0.05 = **.
640
641 **Figure 5. LRA Latency HIV-CRISPR screen identifies ING3 in combination with**
642 **AZD5582 as a HIV-1 latency maintenance factor.**
643 **(A)** *ING3* is the top hit of the LRA Latency HIV-CRISPR screen. The Latency HIV-
644 CRISPR screen HuEpi knockout cells were treated with a low activating dose (10 nM) of
645 AZD5582. The -$\log_{10}$ of the MAGeCK score (on the y-axis) for each gene targeted by
646 the HuEpi sgRNA library (black circles) and NTCs (gray squares) are calculated and
647 displayed. NTCs are artificial NTC genes designed by iterative binning of NTC sgRNA
648 sequences (see Methods). Genes are randomized on the x-axis, but the same order is
649 used for both right and left panels. **(B)** Comparison of the Latency HIV-CRISPR screen
650 by MAGeCK score in the presence (y-axis) and absence of AZD5582 (x-axis) with
651 HuEpi genes (circles) and NTCs (gray squares). The data for the screen without an LRA
652 (x-axis) is from Figure 3 as these two screens were performed in parallel. The genes
653 unique to each screen are closest to the respective axis and the genes that are in
654 common to both screens are at the center. *ING3* is highlighted in periwinkle and *CUL3*
655 in green.
656
657 **Figure 6. Validation of ING3 in combination with AZD5582 as a HIV-1 latency**
658 **maintenance factor.**
659 **(A)** HIV-1 reverse transcriptase activity (y-axis) of the viral supernatant of NTC sgRNA
660 transduction or *ING3* knockout in J-Lat 10.6 and 5A8 treated with 10 nM AZD5582 or an
661 equivalent volume of DMSO. *ING3* knockout and AZD5582 treatment combine to result
662 in a significant increase in viral reactivation. Paired t-test, p-value =<0.05 = *, =<0.05 =
663 **. **(B)** Representative flow cytometry plots of primary CD4+ T cell HIV-1 latency model
664 cells that are *AAVS1* or *ING3* knockouts treated with DMSO or 1 μM AZD5582
665 treatment. Thy1.2-, GFP- cells (quadrant 4) are uninfected; Thy1.2+, GFP- (quadrant 3)
666 cells are infected with the dual reporter HIV-1 virus and latent; Thy1.2+, GFP+ cells
667 (quadrant 2) are infected and reactivated. **(C)** Three independent knockouts of *AAVS1*
668 and *ING3* in primary CD4+ T cell HIV-1 latency model cells were performed in one
669 healthy donor and each pool of knockout cells were treated with DMSO or 1 μM
670 AZD5582 (AZD). Knockout of *ING3* and AZD5582 treatment combined resulted in
671 significant reactivation compared to knockout of *AAVS1*. Paired t-test, p-value =<0.05 =

672 *. **(D)** Western blot showing similar p52 levels are detected in the control and ING3
673 knockout J-Lat 10.6 and 5A8 cell lines upon treatment of 10 nM AZD5582. Activation of
674 the non-canonical NFκB (NFκB2) pathway is marked by a decrease in p100 and an
675 increase in the cleaved product of p52.
676
677 **Figure 7. *ING3* knockout decreases pan-H4Ac and BRD4 levels and stimulates**
678 **HIV-1 transcriptional initiation and elongation upon addition of AZD5582.**
679 **(A)** Genome browser tracks centered over the HIV-1 LTR showing the pan-H4Ac signal
680 decreases in the *ING3* knockout alone and in combination with AZD5582 conditions.
681 The y-axis represents read count. Because the HIV-1 LTR sequence is identical
682 between 5' LTR vs. the 3' LTR, the CUT&Tag reads are combined onto one LTR. The
683 LTR is subdivided into three regions: U3, R (containing the transcription start site), and
684 U5. **(B)** Box plot showing the pan-H4Ac levels quantified over the full LTR including the
685 U3 region and the R+U5 regions that include the transcriptional start site. The y-axis is
686 the pan-H4Ac base pair coverage normalized to the total base pair coverage across the
687 genome. Blue represents the transduction of NTC sgRNA with treatment of DMSO;
688 yellow represents the transduction of NTC sgRNA with a treatment of 10 nM AZD5582;
689 orange represents *ING3* knockout with treatment of DMSO; red represents *ING3*
690 knockout with treatment of 10 nM AZD5582. Replicates for IgG n=18 and pan-H4Ac
691 n=24. For statistical analysis, all conditions are compared to the NTC knockout and
692 DMSO treatment control. P-value <0.05 = *, <0.005=**. **(C)** Genome browser tracks
693 showing BRD4 levels decrease in the *ING3* knockout alone and in combination with
694 AZD5582 conditions. **(D)** Same as (B) but quantifying BRD4 levels. Replicates for BRD4
695 n=16. **(E)** Genome browser tracks showing RNA-Pol2-S5p levels increase at the HIV-1
696 LTR, as well as the body of the provirus downstream of the 5' LTR ("provirus body"),
697 and the region of the host genome downstream of the 3' LTR of the integrated provirus
698 ("downstream") upon *ING3* knockout and AZD5582 treatment combined. **(F)** Box plot
699 showing the quantification of the RNA-Pol2-S5p CUT&Tag signal over the HIV-1 LTR,
700 as well as the body of the provirus, and the region of the host genome downstream of
701 the provirus. The y-axis is the RNA-Pol2-S5p base pair coverage normalized to the total
702 base pair coverage across the genome. Blue represents the transduction of NTC
703 sgRNA with treatment of DMSO; yellow represents the transduction of NTC sgRNA with
704 a treatment of 10 nM AZD5582; orange represents *ING3* knockout with treatment of
705 DMSO; red represents *ING3* knockout with treatment of 10 nM AZD5582. Replicates for
706 RNA-Pol2-S5p n=13. For statistical analysis, all conditions are compared to the NTC
707 knockout and DMSO treatment control. P-value <0.05 = *, <0.005=**, <0.0005=***. **(G)**
708 Genome browser tracks showing RNA-Pol2-S2p levels increase over the body of the
709 HIV-1 provirus as well as the host genome downstream of the provirus upon *ING3*
710 knockout and AZD5582 treatment combined. **(H)** Same as (F) but quantifying RNA-
711 Pol2-S2p levels. Replicates for RNA-Pol2-S2p n=17.
712
713 **Figure 8. Changes in RNA-Pol2-S5p levels upon *ING3* knockout combined with**
714 **AZD5582 treatment are nearly unique to the HIV-1 provirus.**

715 **(A**) Volcano plot comparing RNA-Pol2-S5p peaks between the NTC KO + DMSO
716 (negative control) and ING3 KO + AZD5582 conditions. Highlighted peaks over the HIV-
717 1 LTR (magenta circle), the body of the provirus (purple circle), and downstream region
718 of HIV-1 provirus (teal circle) are the regions of the highest RNA-Pol2-S5p fold change
719 and are highly significant. Other regions with an absolute $\log_2$ fold change greater than 1
720 and a $-\log_{10}$ adjusted p-value > 2 are highlighted in red. **(B)** Scatter plot showing all of
721 the RNA-Pol2-S5p peaks rank ordered by fold change. Peaks are colored as in (A). The
722 top three regions are the HIV-1 LTR, body of the HIV-1 provirus, and downstream
723 region of the HIV-1 provirus. The next two regions overlap *HCG27* and the histone
724 cluster 2 spanning HIST2H4A-HIST2H4B. The region with the greatest reduction in
725 RNA-Pol2-S5p signal overlaps *PCGF3*.
726

727 **Materials and Methods**
728
729 **J-Lat wildtype, clonal knockout, and pooled knockout cells**
730 The HIV-1 latency cell line J-Lat 5A8 [29] and J-Lat 10.6 [28] were grown in RPMI-1640
731 medium (Thermo Fisher Scientific) supplemented with 10% Fetal Bovine Serum (FBS),
732 Penicillin-Streptomycin (Pen/Strep), and 10 mM HEPES. In order to use these cells for
733 screening with HIV-CRISPR, we performed CRISPR/Cas9-mediated knockout of Zinc
734 Antiviral Protein (ZAP) [30] by electroporation of the J-Lat 10.6 and 5A8 cells with a
735 Gene Knockout v2 kit (GKOv2) for ZAP (Synthego, Redwood City, CA) complexed with
736 1 μL of 20 μM Cas9-NLS (UC Berkeley Macro Lab). 5 days post electroporation, the
737 cells were single cell sorted into a 96-well U-bottom plate (Sony MA900 Multi-
738 Application Cell Sorter – Fred Hutch Flow Cytometry shared resource) and individual
739 clones with biallelic knockouts of ZAP were used for subsequent Latency HIV-CRISPR
740 screens. J-Lat cells with HIV-CRISPR KO pools targeting NFKBIA, KAT5, CUL3,
741 ACTL6A, VPS72, DNMT1, DMAP1, SRCAP, YEATS4, and two non-targeting controls
742 (**Supplementary File 1**) were generated by transduction of lentivirus and subsequent
743 0.4 μg/mL puromycin selection for 10-14 days. To generate the CRISPR/Cas9-edited
744 knockout pools, the sgRNAs that were the most overrepresented in the viral
745 supernatant (highest combined p-value) of the Latency HIV-CRISPR screen were
746 selected. Cell lines were determined to be mycoplasma free by the Fred Hutch
747 Specimen Processing/Research Cell Bank shared resource.
748
749 **Plasmids**
750 HIV-CRISPR plasmid was previously described [30]. HIV-CRISPR constructs targeting
751 genes of interest were cloned by annealing complementary oligos (**Supplementary File**
752 **1**) with overhangs that allow directional cloning into HIV-CRISPR using the BsmBI
753 restriction sites. pMD2.G and psPAX2 plasmids were gifts from Didier Trono (Addgene
754 #12259 and #12260, respectively). pMD2.Cocal plasmid was a gift from Hans-Peter
755 Kiem [73]. lentiCRISPRv2 plasmid was a gift from Feng Zhang (Addgene #52961). The
756 pNL4-3-Δ6-dreGFP-CD90 was previously described [50].
757
758 **Human Epigenome CRISPR/Cas9 sgRNA Library Construction**
759 The Human Epigenome (HuEpi) sgRNA library is composed of 841 genes of which 778
760 genes derive from the database Epifactor [32] and 63 genes were hand selected. For
761 most genes, six sgRNA sequences were generated using GUIDES (Graphical User
762 Interface for DNA Editing Screens) [74]. Two genes (HEATR1 and MCM2) have
763 fourteen guides and one gene (UBE2N) has one guide. 252 non-targeting sgRNAs
764 sourced from GeCKO v2.0 library [33] were also included resulting in a generated
765 library of a total of 5,309 guides. The HuEpi sgRNA was synthesized (Twist
766 Biosciences, San Francisco, CA) and cloned into HIV-CRISPR. Oligo pools were
767 amplified using Phusion High-Fidelity DNA Polymerase (NEB) combined with 1 ng of
768 pooled oligo template, primers ArrayF and ArrayR (ArrayF primer:
769 TAACTTGAAAGTATTTCGATTTCTTGGCTTTATATATCTTGTGGAAAGGACGAAACA
770 CCG and ArrayR primer:

771 ACTTTTTCAAGTTGATAACGGACTAGCCTTATTTTAACTTGCTATTTCT
772 AGCTCTAAAAC), an annealing temperature of 59°C, an extension time of 20 s, and 25
773 cycles. Following PCR amplification, a 140 bp amplicon was gel-purified and cloned into
774 BsmBI (NEB; R0580) digested HIVCRISPR using Gibson Assembly (NEB; E2611S).
775 Each Gibson reaction was carried out at 50°C for 60 min. Drop dialysis was performed
776 on each Gibson reaction according to the manufacturer's protocol using a Type-VS
777 Millipore membrane (VSWP 02500). 5 µl of the reaction was used to transform 25 µl of
778 Endura electrocompetent cells (Lucigen; 60242-2) according to the manufacturer's
779 protocol using a Gene Pulser (BioRad). To ensure adequate representation, sufficient
780 parallel transformations were performed and plated onto carbenicillin containing LB
781 agarose 245 mm x 245 mm plates (Thermo Fisher) at 300-times the total number of
782 oligos of each library pool. After overnight growth at 37°C, colonies were scraped off,
783 pelleted, and used for plasmid DNA preps using the Endotoxin-Free Nucleobond
784 Plasmid Midiprep kit (Takara Bio; 740422.10). The HuEpi library was sequenced and
785 contains all 5,309 sgRNAs included in the synthesis (GEO Dataset, submission in
786 progress).
787
788 **Lentivirus Production**
789 293T cells (ATCC;CRL-3216) cultured in DMEM (Thermo Fisher Scientific)
790 supplemented with 10% FBS and PenStrep were plated at 2E5 cells/mL in 2 mL in 6-
791 well plates one day prior to transfection. Transfection is performed using TransIT-LT1
792 reagent (Mirus Bio LLC; MIR2300) with 3 uL of transfection reagent per µg of DNA. For
793 lentiviral preps, 293Ts were transfected with 667 ng lentiviral plasmid, 500 ng psPAX2,
794 and 333 ng pMD2.G. One day post-transfection, media was replaced. Two- or three-
795 days post-transfection, viral supernatants were filtered through a 0.2 µm filter (Thermo
796 Scientific; 720-1320). For HuEpi library lentiviral preps, the same transfection of 293Ts
797 was performed and supernatants from forty 6-well plates were combined and
798 concentrated by ultracentrifugation. About 30 mL of supernatant are aliquoted into a
799 polypropylene tube (Beckman Coulter; 326823) and underlaid with sterile-filtered 20%
800 sucrose (20% sucrose, 1 mM EDTA, 20 mM HEPES, 100 mM NaCl, distilled water).
801 Each of the polypropylene tubes are placed in a swinging bucket and spun in a SW 28
802 rotor at 23,000 rpm for 1 hour at 4°C in a Beckman Coulter Optima L-90K
803 Ultracentrifuge. Supernatants were decanted and pellets are resuspended in DMEM or
804 RPMI over several hours at 4°C. Concentrated lentivirus was used immediately or
805 aliquots were made and stored at -80°C. All lentiviral transductions were performed in
806 the presence of 20 µg/mL DEAE-Dextran (Sigma-Alrdich; D9885). For generating pNL4-
807 3-Δ6-dreGFP-CD90 stocks, the procedure was the same as the lentiviral preps except
808 that 293Ts were transfected with 900 ng lentiviral plasmid, 450 ng psPAX2, and 150 ng
809 pMD2.Cocal.
810
811 **LRA and no LRA Latency HIV-CRISPR Screening**
812 The HuEpi library lentiviral preps were titered by a colony-forming assay in TZM-bl cells
813 (NIH AIDS Reagent Program; ARP-8129) and used to transduce J-Lat 10.6 and J-Lat
814 5A8 cells at an MOI of 0.4. For the transduction, 3E6 cells per replicate (>500x

815 coverage of the HuEpi library) was used and the spinoculation was performed at
816 1100xg for 30 min in the presence of 20 μg/mL DEAE-Dextran. Cells were selected in
817 puromycin (0.4 μg/mL) for 10-14 days. In preparation for the LRA screen, AZD5582
818 dihydrochloride (Tocris; 5141) was resuspended in DMSO to 1 mM stocks. Subsequent
819 dilutions are performed in RPMI and used immediately. Upon completion of selection,
820 for the LRA screen, 3E6 cells per replicate per cell line were treated with 10 nM
821 AZD5582 for 24 hours. Cells and supernatants were collected post selection or post
822 treatment. Cells were washed once with DPBS (Gibco; 14190144) and cell pellets were
823 stored at -20°C. Genomic DNA was extracted from cell pellets with the QIAamp DNA
824 Blood Midi Kit (Qiagen; 51183) and genomic DNA was eluted in distilled water. Viral
825 supernatants were spun at 1100xg to remove cell debris, filtered through a 0.22 μm filter
826 (Millipore Sigma, SE1M179M6), overlaid on a 20% sucrose cushion, and concentrated
827 in a SW 28 rotor for 1 hour at 4°C. The pellet is resuspended in RPMI and stored at -
828 80°C. Viral RNA was extracted from the concentrated virus with the QIAamp Viral RNA
829 Mini Kit (Qiagen, 52904). The sgRNA sequences found in the genomic DNA and viral
830 RNA samples were amplified by PCR (Agilent; 600677) and RT-PCR (Invitrogen;
831 18064014), respectively, using HIV-CRISPR specific primers. A second round of PCR is
832 performed to barcode and prepare the libraries for Illumina sequencing
833 (**Supplementary File 1**). Each amplicon was cleaned up using double-sided bead
834 clean-up (Beckman Coulter; A63880), quantified with a Qubit dsDNA HS Assay Kit
835 (Invitrogen; Q32854), and pooled to 10 nM for each library. Library pools are sequenced
836 on a single lane of an Illumina HiSeq 2500 in Rapid Run mode (Fred Hutch Genomics
837 and Bioinformatics shared resource).
838
839 **Screen Analysis**
840 Raw sequencing data is available as a GEO DataSet (submission in progress). Library
841 pools are demultiplexed, reads are assigned to respective samples, trimmed, and
842 aligned to the HuEpi library via Bowtie [75]. An artificial NTC sgRNA gene set the same
843 size as the HuEpi library was generated by iteratively binning the NTC sgRNA
844 sequences. Analysis of the screen to determine relative enrichment or depletion of the
845 sgRNAs and genes were performed using the MAGeCK statistical package [35].
846
847 **Western Blotting/Immunoblotting**
848 Cells were harvested and washed once with ice cold phosphate-buffered saline (PBS)
849 and pelleted by centrifugation (300 x g for 3 min). Whole cell lysate was extracted on ice
850 by first resuspending the cell pellet with Pierce IP Lysis Buffer (ThermoFisher Scientific;
851 87787) supplemented with cOmplete protease inhibitor cocktail (Roche; 11697498001).
852 The samples were then incubated on ice for 10 min with brief vortexing every 2-3 min
853 and followed by a centrifugation at 16,000 x g for 20 min at 4°C. To prepare the
854 samples, add 4x NuPAGE LDS Sample Buffer (ThermoFisher Scientific; NP0008)
855 containing 5% 2-Mercaptoethanol (Millipore Sigma; M3148) and boil the samples at
856 95°C for 5 min. Lysates were resolved on a NuPAGE 4-12% Bis-Tris pre-cast gel
857 (ThermoFisher Scientific; NP0336) and transferred to nitrocellulose membranes (Biorad;
858 1620115). Blocking was performed for 1 hr at room temperature using 5% milk/0.1%

859 Tween-20 added to Tris-buffered saline (TBS) (20 mM Tris base and 150 mM NaCl at
860 pH 7.6). Immunoblotting was performed using the primary antibodies CUL3 (Cell
861 Signaling; 2759) at 1:1000, NFkB2 (Cell Signaling; 4882) at 1:1000, and viniculin (Santa
862 Cruz; sc-25336) at 1:5000. Membranes were washed with TBST 6 times for 5 min each.
863 The following secondary antibodies were used at a 1:5000 dilution: goat anti-rabbit IgG-
864 HRP (R&D Systems; HAF008) and goat anti-mouse IgG-HRP (R&D Systems; HAF007).
865 Membranes were developed with SuperSignal West Femto Maximum Sensitivity
866 Substrate (Thermo Fisher; 34095) and visualized on a BioRad Chemidoc MP Imaging
867 System.
868
869 **Genomic Editing Analysis**
870 Knockout cells were harvested and DNA was extracted using the QIAamp DNA Blood
871 Mini Kit (Qiagen; 51104). Primers from each targeted locus (Supplementary File 1) were
872 used to amplify the edited loci and the PCR was performed with either Platinum Taq
873 DNA Polymerase High Fidelity (ThermoFisher Scientific; 11304011) or Q5 High-Fidelity
874 DNA Polymerase (NEB; M0491S). Sanger sequencing was performed on PCR
875 amplicons (Fred Hutch Genomics shared resource) using a sequencing primer
876 (Supplementary File 1) and results were analyzed by Inference of CRISPR Edits (ICE)
877 [44] to determine gene editing outcome.
878
879 **Virus Release (RT assay)**
880 Clarified viral supernatants are harvested and reverse transcriptase activity was
881 measured using the HIV-1 reverse transcriptase (RT) activity assay as previously
882 described [76, 77]. A standard curve is generated for all assays using a titered stock of
883 HIV-1_{LAI} that was aliquoted at and stored at -80°C.
884
885 **Ethics Statement**
886 All primary cell data is from anonymous blood donors and is classified as "human
887 subjects exempt" research by the Fred Hutchinson Cancer Center Institutional Review
888 Boards, according to National Institutes of Health (NIH) guidelines
889 (http://grants.nih.gov/grants/policy/hs/faqs_aps_definitions.htm). No animal work was
890 done.
891
892 **Primary CD4+ T Cell Latency Model and Knockout**
893 Used leukocyte filters from healthy donors were obtained from Bloodworks Northwest
894 and total peripheral blood mononuclear cells (PBMCs) were isolated by purification over
895 Ficoll (Millipore Sigma; GE17-1440-02). CD4+ T cells were isolated using magnetic
896 negative selection (StemCell Technologies; 17952) and used immediately or frozen for
897 storage in liquid nitrogen. CD4+ T cells were activated using anti-CD2, CD3, and CD28
898 beads (Miltenyi Biotec; 130-091-441) for 2 days and grown in RPMI-1640 medium
899 (Thermo Fisher Scientific) supplemented with 10% Fetal Bovine Serum (FBS),
900 Penicillin-Streptomycin (Pen/Strep), 1x GlutaMAX (ThermoFisher Scientific; 35050061),
901 10 mM HEPES, 100 U/mL human interleukin-2 (Millipore Sigma; 11011456001), 2
902 ng/mL human interleukin-7 (Peptrotech; 200-07), and 2 ng/mL human interleukin-15

903 (Peprotech; 200-15). The beads were then removed by magnetic separation and cells
904 were spinoculated with HIV-GFP-Thy1.2 (pNL4-3-Δ6-dreGFP-CD90) and 8 ug/mL
905 polybrene (Millipore Sigma; TR-1003-G) for 2 hrs at 1100 x g. Spinoculated cells were
906 then resuspended in fresh media with IL-2, IL-7, and IL-15 and incubated for 3 days
907 before actively infected cells (Thy1.2+) were isolated by magnetic positive selection
908 (Stem Cell Technologies; 18951). Infected cells (Thy1.2+) are maintained for 2 days
909 before knockout of AAVS1, CUL3, and ING3 using GKOv2 kits from Synthego. crRNPs
910 for each gene of interest were generated as described previously in the Knockout Cell
911 Clones and Pools section except that supplemented P3 buffer (Lonza; V4SP-3096) is
912 used instead of SE buffer. For each electroporation, 1.5E6 cells were pelleted by
913 centrifugation at 100 x g for 10 min at 25°C, washed once with PBS, pelleted again by
914 centrifugation, PBS was removed, and resuspended with a crRNP complex. The
915 resuspended cells were immediately transferred into the cuvette of the P3 Primary Cell
916 Nucleofector Kit (Lonza; V4SP-3096) and electroporated using code EH-100 on the
917 Lonza 4D-Nucleofector. 80 μL of prewarmed supplemented RPMI media with IL-2, IL-7,
918 and IL-15 was added and cells were allowed to recover for 10 min in the 37°C
919 incubator. 300 μL of fresh media was added and cells are transferred to a 96-well plate.
920 200 μL of additional supplemented media was added 2 days later. The knockout cells
921 are maintained at 1E6 cells/mL with fresh media supplemented with IL-2, IL-7, and IL-
922 15. At 14 days post infection, cells are co-cultured with H80 feeder cells and maintained
923 at 2E6 cells/mL in media supplemented with 20 U/mL IL-2. If AZD5582 treatment
924 applies, cells are treated 1 uM AZD5582 media for 24 hours. At 19 days post infection,
925 cells were stained with Thy1.2 antibody (Biolegend; 140323), fixed with 4% PFA, and
926 underwent flow cytometry analysis (CD FACS Celesta – Fred Hutch Flow Cytometry
927 shared resource).
928
929 **Automated CUT&Tag Profiling**
930 We prepared nuclei from J-Lat 10.6 cells under four conditions: (i) NTC knockout with a
931 treatment of DMSO (negative control) (ii) NTC knockout with a treatment of 10 nM
932 AZD5582 (iii) ING3 knockout with a treatment of DMSO (iv) ING3 knockout with a
933 treatment of 10 nM AZD5582. Up to 10 million cells were pelleted in 1.5 mL microfuge
934 tubes spun at 300 x g for 10 min. Cells were then resuspended in 1 mL of ice cold NE1
935 Buffer (20 mM HEPES-KOH pH 7.9, 10 mM KCl, 0.5 mM Spermidine, 0.1% TritonX-
936 100, 20% Glycerol, with Roche complete EDTA-free protease inhibitor tablet), and
937 incubated on ice for 10 min. Nuclei were then centrifuged at 4°C at 1,300 x g for 4 min.
938 Nuclei were then resuspended in 1 mL of Wash Buffer (20 mM HEPES pH7.5, 150 mM
939 NaCl, 0.5 mM spermidine, supplemented with Roche complete EDTA-free protease
940 inhibitor tablet). 10 μL was used to determine the concentration of native J-Lat 10.6
941 nuclei, and nuclei were diluted to a concentration of 1 million nuclei/900 μL of Wash
942 Buffer and 900 μL aliquots of this suspension was mixed with 100 μL of DMSO in
943 Cryovials, which were then sealed and placed inside a Mr. Frosty isopropanol chamber
944 for slow freezing at -80°C. Nuclei were then stored at -80°C until use. For automated
945 CUT&Tag processing, nuclei were thawed at room temperature, washed in wash buffer,
946 and bound to concanvalin-A (ConA) paramagnetic beads (Bangs Laboratories; BP531)

947 for magnetic separation as described on the protocols.io website
948 (https://doi.org/10.17504/protocols.io.bgztjx6n).Samples were then suspended in
949 antibody binding buffer and split for overnight incubation with antibodies specific to
950 panH4Ac (Active Motif; 39925), BRD4 (Cell Signaling; 13440), RNA-Pol2-S5p (Cell
951 Signaling; 13523), RNA-Pol2-S2p (Cell Signaling; 13499), and IgG control(Abcam;
952 172730). Sample processing was performed in a 96 well plate using 100K Con-A bound
953 nuclei per reaction on a Beckman Coulter Biomek liquid handling robot according to the
954 AutoCUT&Tag protocol available from the protocols.io website
955 (https://doi.org/10.17504/protocols.io.bgztjx6n) and described previously [31] (Fred
956 Hutch Genomics shared resource).
957
958 **CUT&Tag Sequencing Data Processing and Analysis**
959 For AutoCUT&Tag sample pooling and sequencing, the size distribution and molar
960 concentration of libraries were determined using an Agilent 4200 TapeStation, and up to
961 96 barcoded CUT&Tag libraries were pooled at approximately equimolar concentration
962 for sequencing. Paired-end 2 × 50 bp sequencing was performed on the NextSeq 2000
963 platform by the Fred Hutchinson Cancer Research Center Genomics Shared
964 Resources. This yielded 5–10 million reads per antibody. Sequences the extended into
965 the 3' adapter were first removed using the adapter clipping tool by cutadapt 2.9 with
966 parameters:
967 -j 8 --nextseq-trim 20 -m 20 -a AGATCGGAAGAGCACACGTCTGAACTCCAGTCA -A
968 AGATCGGAAGAGCGTCGTGTAGGGAAAGAGTGT -Z.
969 To construct a reference reflecting integration of HIV-1 into J-Lat cells, we started with
970 the UCSC hg38 human reference sequence from the Illumina iGenomes collection
971 (https://support.illumina.com/sequencing/sequencing_software/igenome.html).
972 Sequence for the integrated HIV-1 genome, including flanking human sequence, was
973 obtained from accession MN989412.1 [78]. Accounting for flanking human sequence,
974 we excised chr9:136468439-136468594 from the reference Fasta file and inserted
975 MN989412.1 in its place. We also rewrote gene & exon annotations downstream of the
976 integration site, shifting all features in the associated GTF file by 10206bp to account for
977 newly inserted HIV-1 sequence. Indexes for Bowtie2 v2.4.1 [79] and STAR v2.7.7a [80]
978 were built using these modified Fasta and GTF files. The HIV-1 insertion is bounded by
979 a pair of LTRs that, because they comprise identical sequence, are difficult for some
980 alignment programs to interpret. To avoid these difficulties when needed, another
981 version of the reference sequence was prepared with the second copy of the LTR
982 sequence (634bp) masked by 'N's.
983 Fastq files were aligned to the custom hg38 genome with the HIV-1 genome inserted in
984 chromosome 9 using Bowtie2 version 2.4.2 with the following parameters: --very-
985 sensitive-local --soft-clipped-unmapped-tlen --dovetail --no-mixed --no-discordant -q --
986 phred33 -I 10 -X 1000. Raw sequencing data is available as a GEO DataSet
987 (submission in progress). Because the read depth and fraction of PCR duplicates varied
988 considerably between replicates, we removed all duplicate reads from the Bed files.
989 Peak calling was performed for the BRD4, pan-H4ac, RNA-Pol2-S5p, and RNA-Pol2-
990 S2p data sets on the pooled reads from all replicates and all conditions using SEACR

991 version 1.3 [81]. We called peaks using two settings, (1) in which using the IgG control
992 data with stringent settings, and (2) using a FDR of 0.01, and then used the FDR 0.01
993 peaks that overlapped with IgG peaks as our final peak set. For correlation analysis
994 between replicates, the BRD4 peak set was merged with the pan-H4ac peak set, and
995 the RNA-Pol2-S5p peak set was merged with the RNA-Pol2-S2p peak set. For
996 statistical comparisons presented in Figure 7, we quantified the base pair coverage of
997 pan-H4ac or BRD4 over the LTR, the U3 region, or the R + U5 region and these values
998 were normalized to the total base pair coverage across the genome for each replicate.
999 Similarly, for comparisons of the RNA-Pol2-S5p data and RNA-Pol2-S2p data, we
1000 quantified the base pair coverage over the LTR, Provirus Body, and Downstream
1001 Region of the HIV provirus these values were normalized to the total base pair coverage
1002 across the genome for each replicate. For comparisons in Figure 7, p-values were
1003 calculated using a two-sample t tests (two sided) with the SciPy.stats.ttest_ind() function
1004 in Python; P values were not corrected for multiple-hypothesis testing. For global
1005 comparison of RNA-Pol2-S5p data between the NTC + DMSO condition and the ING
1006 KO + AZD5582 condition, presented in Figure 8, reads that overlapped RNA-Pol2-S5p
1007 peaks were counted for each replicate and the log 2 Fold Change and adjusted p-
1008 values were calculated using DESeq2 version 1.32.0 using the Wald test. The adjusted
1009 p-values are corrected for multiple-hypothesis testing in a manner that is proportional to
1010 the number of RNA-Pol2-S5p peaks. DESeq2 assigns peaks with extremely sparse
1011 data are assigned an adjusted p-value of NaN, and these peaks were excluded form
1012 downstream analysis.

1013 **References**

1014 1. Deeks, S.G., et al., *HIV infection.* Nat Rev Dis Primers, 2015. **1**: p. 15035.
1015 2. Chun, T.W., et al., *Re-emergence of HIV after stopping therapy.* Nature, 1999. **401**(6756):
1016 p. 874-5.
1017 3. Finzi, D., et al., *Latent infection of CD4+ T cells provides a mechanism for lifelong*
1018 *persistence of HIV-1, even in patients on effective combination therapy.* Nat Med, 1999.
1019 **5**(5): p. 512-7.
1020 4. Sengupta, S. and R.F. Siliciano, *Targeting the Latent Reservoir for HIV-1.* Immunity, 2018.
1021 **48**(5): p. 872-895.
1022 5. Einkauf, K.B., et al., *Intact HIV-1 proviruses accumulate at distinct chromosomal*
1023 *positions during prolonged antiretroviral therapy.* J Clin Invest, 2019. **129**(3): p. 988-998.
1024 6. Jiang, C., et al., *Distinct viral reservoirs in individuals with spontaneous control of HIV-1.*
1025 Nature, 2020. **585**(7824): p. 261-267.
1026 7. Mbonye, U. and J. Karn, *The Molecular Basis for Human Immunodeficiency Virus*
1027 *Latency.* Annu Rev Virol, 2017. **4**(1): p. 261-285.
1028 8. Turner, A.W., et al., *Evaluation of EED Inhibitors as a Class of PRC2-Targeted Small*
1029 *Molecules for HIV Latency Reversal.* ACS Infect Dis, 2020. **6**(7): p. 1719-1733.
1030 9. Li, Z., et al., *The KAT5-Acetyl-Histone4-Brd4 axis silences HIV-1 transcription and*
1031 *promotes viral latency.* PLoS Pathog, 2018. **14**(4): p. e1007012.
1032 10. Nguyen, K., et al., *Multiple Histone Lysine Methyltransferases Are Required for the*
1033 *Establishment and Maintenance of HIV-1 Latency.* mBio, 2017. **8**(1).
1034 11. Nixon, C.C., et al., *Systemic HIV and SIV latency reversal via non-canonical NF-kappaB*
1035 *signalling in vivo.* Nature, 2020. **578**(7793): p. 160-165.
1036 12. Margolis, D.M., et al., *Curing HIV: Seeking to Target and Clear Persistent Infection.* Cell,
1037 2020. **181**(1): p. 189-206.
1038 13. Turner, A.W. and D.M. Margolis, *Chromatin Regulation and the Histone Code in HIV*
1039 *Latency.* Yale J Biol Med, 2017. **90**(2): p. 229-243.
1040 14. Boehm, D. and M. Ott, *Host Methyltransferases and Demethylases: Potential New*
1041 *Epigenetic Targets for HIV Cure Strategies and Beyond.* AIDS Res Hum Retroviruses,
1042 2017. **33**(S1): p. S8-s22.
1043 15. Li, Z., et al., *The BET bromodomain inhibitor JQ1 activates HIV latency through*
1044 *antagonizing Brd4 inhibition of Tat-transactivation.* Nucleic Acids Res, 2013. **41**(1): p.
1045 277-87.
1046 16. Bisgrove, D.A., et al., *Conserved P-TEFb-interacting domain of BRD4 inhibits HIV*
1047 *transcription.* Proc Natl Acad Sci U S A, 2007. **104**(34): p. 13690-5.
1048 17. Conrad, R.J., et al., *The Short Isoform of BRD4 Promotes HIV-1 Latency by Engaging*
1049 *Repressive SWI/SNF Chromatin-Remodeling Complexes.* Mol Cell, 2017. **67**(6): p. 1001-
1050 1012.e6.
1051 18. Friedman, J., et al., *Epigenetic silencing of HIV-1 by the histone H3 lysine 27*
1052 *methyltransferase enhancer of Zeste 2.* J Virol, 2011. **85**(17): p. 9078-89.
1053 19. Tripathy, M.K., et al., *H3K27 Demethylation at the Proviral Promoter Sensitizes Latent*
1054 *HIV to the Effects of Vorinostat in Ex Vivo Cultures of Resting CD4+ T Cells.* J Virol, 2015.
1055 **89**(16): p. 8392-405.

1056 20. Besnard, E., et al., *The mTOR Complex Controls HIV Latency.* Cell Host Microbe, 2016.
1057 **20**(6): p. 785-797.
1058 21. Das, B., et al., *Estrogen receptor-1 is a key regulator of HIV-1 latency that imparts*
1059 *gender-specific restrictions on the latent reservoir.* Proc Natl Acad Sci U S A, 2018.
1060 **115**(33): p. E7795-e7804.
1061 22. Boehm, D., et al., *SMYD2-Mediated Histone Methylation Contributes to HIV-1 Latency.*
1062 Cell Host Microbe, 2017. **21**(5): p. 569-579.e6.
1063 23. Li, Z., et al., *Reiterative Enrichment and Authentication of CRISPRi Targets (REACT)*
1064 *identifies the proteasome as a key contributor to HIV-1 latency.* PLoS Pathog, 2019.
1065 **15**(1): p. e1007498.
1066 24. Huang, H., et al., *A CRISPR/Cas9 screen identifies the histone demethylase MINA53 as a*
1067 *novel HIV-1 latency-promoting gene (LPG).* Nucleic Acids Res, 2019. **47**(14): p. 7333-
1068 7347.
1069 25. Rathore, A., et al., *CRISPR-based gene knockout screens reveal deubiquitinases involved*
1070 *in HIV-1 latency in two Jurkat cell models.* Sci Rep, 2020. **10**(1): p. 5350.
1071 26. Pedersen, S.F., et al., *Inhibition of a Chromatin and Transcription Modulator, SLTM,*
1072 *Increases HIV-1 Reactivation Identified by a CRISPR Inhibition Screen.* J Virol, 2022: p.
1073 e0057722.
1074 27. Pache, L., et al., *BIRC2/cIAP1 Is a Negative Regulator of HIV-1 Transcription and Can Be*
1075 *Targeted by Smac Mimetics to Promote Reversal of Viral Latency.* Cell Host Microbe,
1076 2015. **18**(3): p. 345-53.
1077 28. Jordan, A.B., D.; Verdin, E., *HIV reproducibly establishes a latent infection after acute*
1078 *infection of T cells in vitro.* The EMBO Journal, 2003. **22**: p. 1868-1877.
1079 29. Chan, J.K., et al., *Calcium/calcineurin synergizes with prostratin to promote NF-kappaB*
1080 *dependent activation of latent HIV.* PLoS One, 2013. **8**(10): p. e77749.
1081 30. OhAinle, M., et al., *A virus-packageable CRISPR screen identifies host factors mediating*
1082 *interferon inhibition of HIV.* Elife, 2018. **7**.
1083 31. Janssens, D.H., et al., *Automated CUT&Tag profiling of chromatin heterogeneity in*
1084 *mixed-lineage leukemia.* Nat Genet, 2021. **53**(11): p. 1586-1596.
1085 32. Medvedeva, Y.A., et al., *EpiFactors: a comprehensive database of human epigenetic*
1086 *factors and complexes.* Database, 2015. **2015**.
1087 33. Sanjana, N.E., O. Shalem, and F. Zhang, *Improved vectors and genome-wide libraries for*
1088 *CRISPR screening.* Nat Methods, 2014. **11**(8): p. 783-784.
1089 34. Spina, C.A., et al., *An in-depth comparison of latent HIV-1 reactivation in multiple cell*
1090 *model systems and resting CD4+ T cells from aviremic patients.* PLoS Pathog, 2013.
1091 **9**(12): p. e1003834.
1092 35. Li, W., et al., *MAGeCK enables robust identification of essential genes from genome-*
1093 *scale CRISPR/Cas9 knockout screens.* Genome Biology, 2014. **15**(12): p. 554.
1094 36. Yang, Z., et al., *Recruitment of P-TEFb for stimulation of transcriptional elongation by the*
1095 *bromodomain protein Brd4.* Mol Cell, 2005. **19**(4): p. 535-45.
1096 37. Doyon, Y., et al., *Structural and functional conservation of the NuA4 histone*
1097 *acetyltransferase complex from yeast to humans.* Mol Cell Biol, 2004. **24**(5): p. 1884-96.

1098 38. Ginsburg, D.S., C.K. Govind, and A.G. Hinnebusch, *NuA4 lysine acetyltransferase Esa1 is*
1099 *targeted to coding regions and stimulates transcription elongation with Gcn5.* Mol Cell
1100 Biol, 2009. **29**(24): p. 6473-87.
1101 39. Doyon, Y. and J. Côté, *The highly conserved and multifunctional NuA4 HAT complex.* Curr
1102 Opin Genet Dev, 2004. **14**(2): p. 147-54.
1103 40. Ruhl, D.D., et al., *Purification of a human SRCAP complex that remodels chromatin by*
1104 *incorporating the histone variant H2A.Z into nucleosomes.* Biochemistry, 2006. **45**(17): p.
1105 5671-7.
1106 41. Mizuguchi, G., et al., *ATP-driven exchange of histone H2AZ variant catalyzed by SWR1*
1107 *chromatin remodeling complex.* Science, 2004. **303**(5656): p. 343-8.
1108 42. Luk, E., et al., *Stepwise histone replacement by SWR1 requires dual activation with*
1109 *histone H2A.Z and canonical nucleosome.* Cell, 2010. **143**(5): p. 725-36.
1110 43. Zhou, Y., et al., *Metascape provides a biologist-oriented resource for the analysis of*
1111 *systems-level datasets.* Nat Commun, 2019. **10**(1): p. 1523.
1112 44. Hsiau, T., et al., *Inference of CRISPR Edits from Sanger Trace Data.* bioRxiv, 2019: p.
1113 251082.
1114 45. Hiatt, J., et al., *A functional map of HIV-host interactions in primary human T cells.* Nat
1115 Commun, 2022. **13**(1): p. 1752.
1116 46. Rountree, M.R., K.E. Bachman, and S.B. Baylin, *DNMT1 binds HDAC2 and a new co-*
1117 *repressor, DMAP1, to form a complex at replication foci.* Nat Genet, 2000. **25**(3): p. 269-
1118 77.
1119 47. Pintard, L., A. Willems, and M. Peter, *Cullin-based ubiquitin ligases: Cul3-BTB complexes*
1120 *join the family.* Embo j, 2004. **23**(8): p. 1681-7.
1121 48. Jefferys, S.R., et al., *Epigenomic characterization of latent HIV infection identifies latency*
1122 *regulating transcription factors.* PLoS Pathog, 2021. **17**(2): p. e1009346.
1123 49. Yang, H.C., et al., *Small-molecule screening using a human primary cell model of HIV*
1124 *latency identifies compounds that reverse latency without cellular activation.* J Clin
1125 Invest, 2009. **119**(11): p. 3473-86.
1126 50. Peterson, J.J., et al., *A histone deacetylase network regulates epigenetic reprogramming*
1127 *and viral silencing in HIV infected cells.* bioRxiv, 2022: p. 2022.05.09.491199.
1128 51. Chu, V.T., et al., *Increasing the efficiency of homology-directed repair for CRISPR-Cas9-*
1129 *induced precise gene editing in mammalian cells.* Nat Biotechnol, 2015. **33**(5): p. 543-8.
1130 52. Langer, S., et al., *The E3 Ubiquitin-Protein Ligase Cullin 3 Regulates HIV-1 Transcription.*
1131 Cells, 2020. **9**(9).
1132 53. Doyon, Y., et al., *ING tumor suppressor proteins are critical regulators of chromatin*
1133 *acetylation required for genome expression and perpetuation.* Mol Cell, 2006. **21**(1): p.
1134 51-64.
1135 54. Hsin, J.P. and J.L. Manley, *The RNA polymerase II CTD coordinates transcription and RNA*
1136 *processing.* Genes Dev, 2012. **26**(19): p. 2119-37.
1137 55. Czudnochowski, N., C.A. Bösken, and M. Geyer, *Serine-7 but not serine-5*
1138 *phosphorylation primes RNA polymerase II CTD for P-TEFb recognition.* Nat Commun,
1139 2012. **3**: p. 842.

1140 56. Ravens, S., et al., *Tip60 complex binds to active Pol II promoters and a subset of*
1141 *enhancers and co-regulates the c-Myc network in mouse embryonic stem cells.*
1142 Epigenetics Chromatin, 2015. **8**: p. 45.
1143 57. Devoucoux, M., et al., *Oncogenic ZMYND11-MBTD1 fusion protein anchors the*
1144 *NuA4/TIP60 histone acetyltransferase complex to the coding region of active genes.* Cell
1145 Rep, 2022. **39**(11): p. 110947.
1146 58. Li, J., et al., *ZMYND11-MBTD1 induces leukemogenesis through hijacking NuA4/TIP60*
1147 *acetyltransferase complex and a PWWP-mediated chromatin association mechanism.*
1148 Nat Commun, 2021. **12**(1): p. 1045.
1149 59. Auger, A., et al., *Eaf1 is the platform for NuA4 molecular assembly that evolutionarily*
1150 *links chromatin acetylation to ATP-dependent exchange of histone H2A variants.* Mol
1151 Cell Biol, 2008. **28**(7): p. 2257-70.
1152 60. Ott, M., et al., *Acetylation of the HIV-1 Tat protein by p300 is important for its*
1153 *transcriptional activity.* Curr Biol, 1999. **9**(24): p. 1489-92.
1154 61. Lusic, M., et al., *Regulation of HIV-1 gene expression by histone acetylation and factor*
1155 *recruitment at the LTR promoter.* Embo j, 2003. **22**(24): p. 6550-61.
1156 62. Van Lint, C., et al., *Transcriptional activation and chromatin remodeling of the HIV-1*
1157 *promoter in response to histone acetylation.* Embo j, 1996. **15**(5): p. 1112-20.
1158 63. Benkirane, M., et al., *Activation of integrated provirus requires histone*
1159 *acetyltransferase. p300 and P/CAF are coactivators for HIV-1 Tat.* J Biol Chem, 1998.
1160 **273**(38): p. 24898-905.
1161 64. Hottiger, M.O. and G.J. Nabel, *Interaction of human immunodeficiency virus type 1 Tat*
1162 *with the transcriptional coactivators p300 and CREB binding protein.* J Virol, 1998.
1163 **72**(10): p. 8252-6.
1164 65. Marzio, G., et al., *HIV-1 tat transactivator recruits p300 and CREB-binding protein*
1165 *histone acetyltransferases to the viral promoter.* Proc Natl Acad Sci U S A, 1998. **95**(23):
1166 p. 13519-24.
1167 66. Col, E., et al., *The histone acetyltransferase, hGCN5, interacts with and acetylates the*
1168 *HIV transactivator, Tat.* J Biol Chem, 2001. **276**(30): p. 28179-84.
1169 67. Steger, D.J., et al., *Purified histone acetyltransferase complexes stimulate HIV-1*
1170 *transcription from preassembled nucleosomal arrays.* Proc Natl Acad Sci U S A, 1998.
1171 **95**(22): p. 12924-9.
1172 68. Falcinelli, S.D., et al., *Combined noncanonical NF-κB agonism and targeted BET*
1173 *bromodomain inhibition reverse HIV latency ex vivo.* J Clin Invest, 2022. **132**(8).
1174 69. Schröder, A.R., et al., *HIV-1 integration in the human genome favors active genes and*
1175 *local hotspots.* Cell, 2002. **110**(4): p. 521-9.
1176 70. Almeida, M., et al., *PCGF3/5-PRC1 initiates Polycomb recruitment in X chromosome*
1177 *inactivation.* Science, 2017. **356**(6342): p. 1081-1084.
1178 71. Sharma, A.L., et al., *CBF-1 Promotes the Establishment and Maintenance of HIV Latency*
1179 *by Recruiting Polycomb Repressive Complexes, PRC1 and PRC2, at HIV LTR.* Viruses,
1180 2020. **12**(9).
1181 72. Gonçalves, E., et al., *Minimal genome-wide human CRISPR-Cas9 library.* Genome Biol,
1182 2021. **22**(1): p. 40.

1183 73. Humbert, O., et al., *Development of Third-generation Cocal Envelope Producer Cell Lines*
1184 *for Robust Lentiviral Gene Transfer into Hematopoietic Stem Cells and T-cells.* Mol Ther,
1185 2016. **24**(7): p. 1237-46.
1186 74. Meier, J.A., F. Zhang, and N.E. Sanjana, *GUIDES: sgRNA design for loss-of-function*
1187 *screens.* Nat Methods, 2017. **14**(9): p. 831-832.
1188 75. Langmead, B., et al., *Ultrafast and memory-efficient alignment of short DNA sequences*
1189 *to the human genome.* Genome Biol, 2009. **10**(3): p. R25.
1190 76. Roesch, F., M. OhAinle, and M. Emerman, *A CRISPR screen for factors regulating*
1191 *SAMHD1 degradation identifies IFITMs as potent inhibitors of lentiviral particle delivery.*
1192 Retrovirology, 2018. **15**(1): p. 26.
1193 77. Vermeire, J., et al., *Quantification of reverse transcriptase activity by real-time PCR as a*
1194 *fast and accurate method for titration of HIV, lenti- and retroviral vectors.* PLoS One,
1195 2012. **7**(12): p. e50859.
1196 78. Chung, C.H., et al., *Integrated Human Immunodeficiency Virus Type 1 Sequence in J-Lat*
1197 *10.6.* Microbiol Resour Announc, 2020. **9**(18).
1198 79. Langmead, B. and S.L. Salzberg, *Fast gapped-read alignment with Bowtie 2.* Nat
1199 Methods, 2012. **9**(4): p. 357-9.
1200 80. Dobin, A., et al., *STAR: ultrafast universal RNA-seq aligner.* Bioinformatics, 2013. **29**(1):
1201 p. 15-21.
1202 81. Meers, M.P., D. Tenenbaum, and S. Henikoff, *Peak calling by Sparse Enrichment Analysis*
1203 *for CUT&RUN chromatin profiling.* Epigenetics Chromatin, 2019. **12**(1): p. 42.
1204

1205

Figure 1

A

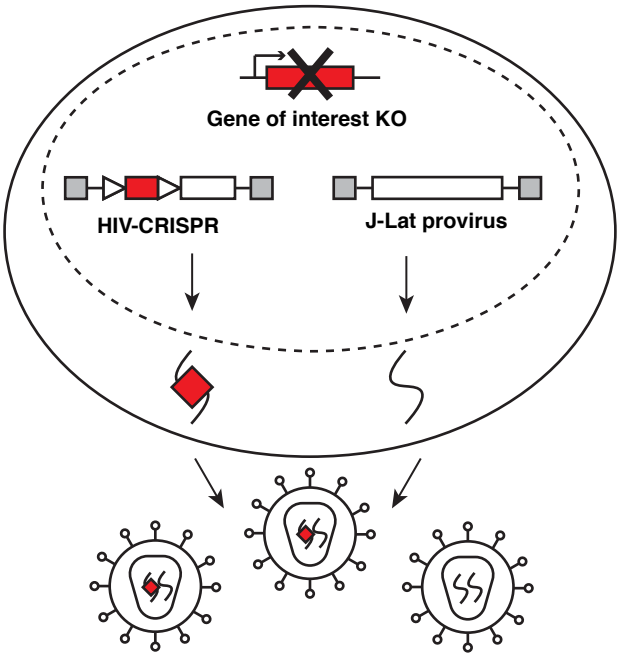

D

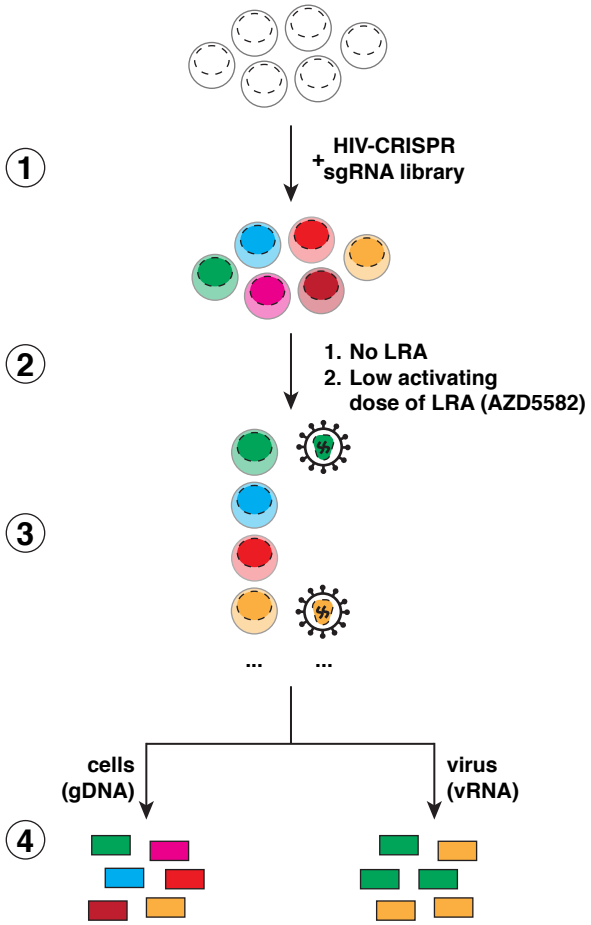

B

	Number of Genes
Histones	84
Histone binders	128
Histone modifiers	365
General chromatin associated	221
Other	43

C

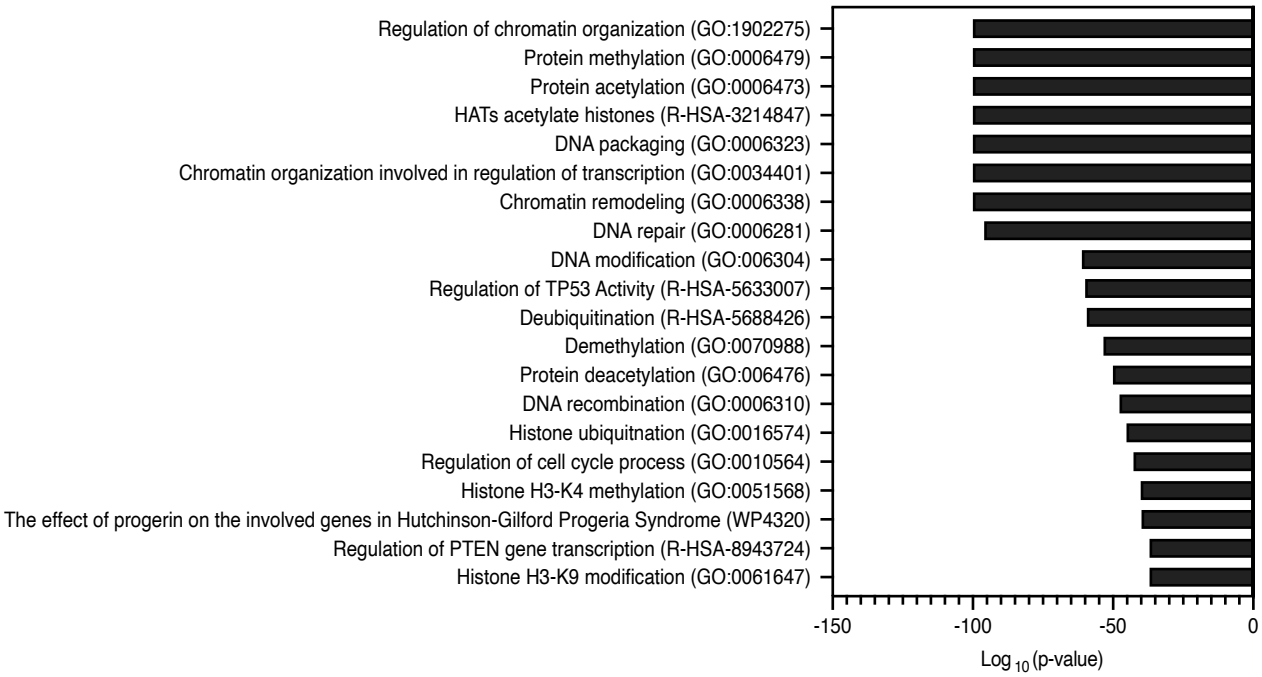

Figure 2

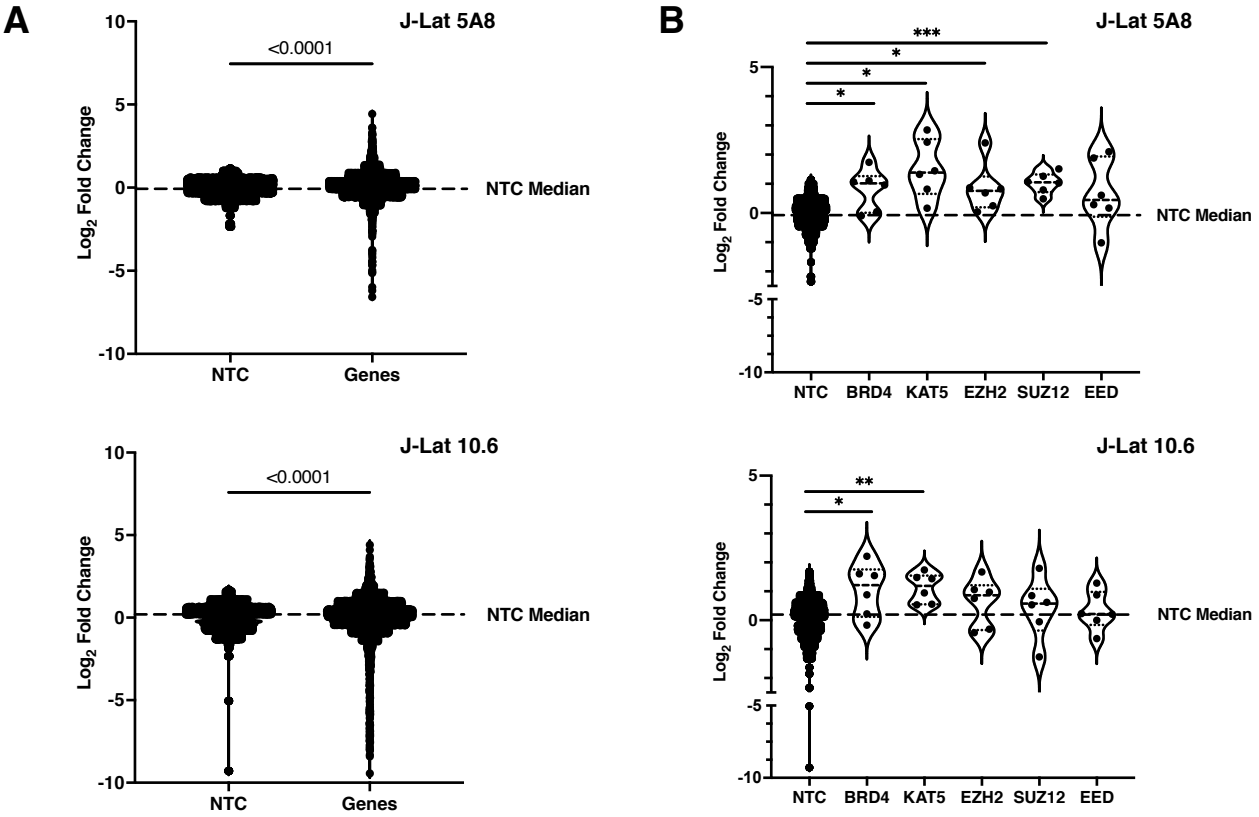
A
J-Lat 5A8
<0.0001
Log2 Fold Change
NTC Median
NTC
Genes
J-Lat 10.6
<0.0001
Log2 Fold Change
NTC Median
NTC
Genes
B
J-Lat 5A8
***
*
*
*
Log2 Fold Change
NTC Median
NTC
BRD4
KAT5
EZH2
SUZ12
EED
J-Lat 10.6
**
*
Log2 Fold Change
NTC Median
NTC
BRD4
KAT5
EZH2
SUZ12
EED

Figure 3

A

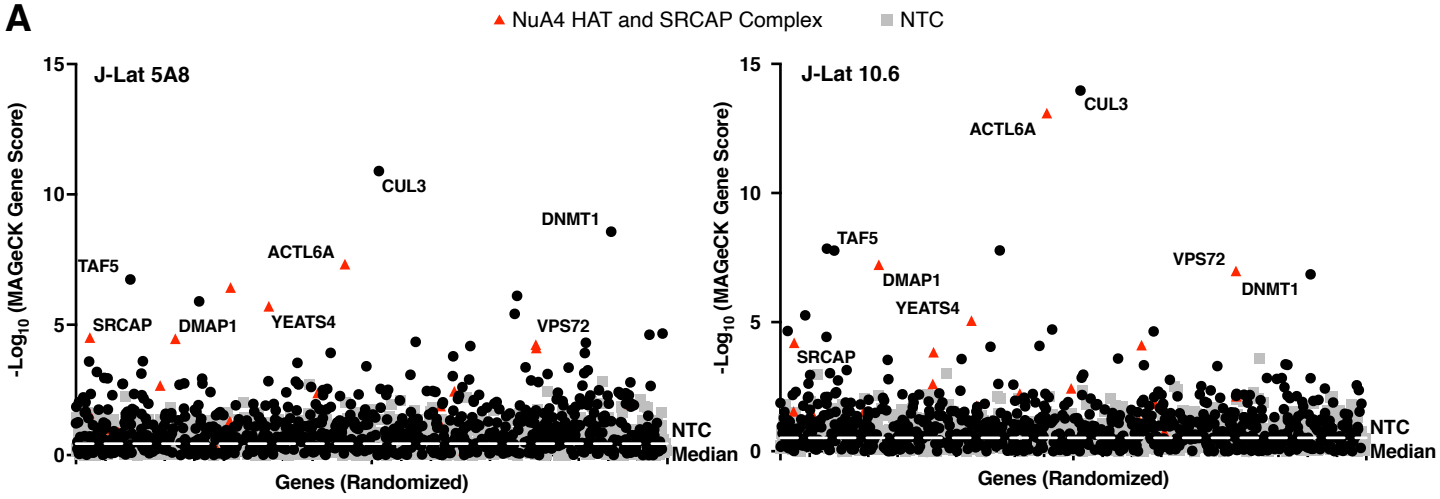

B

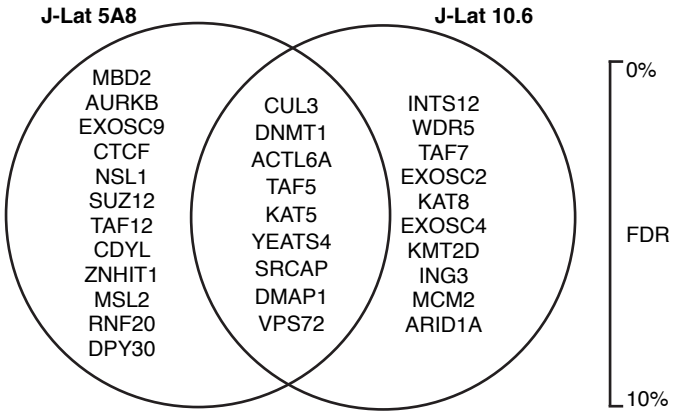

C

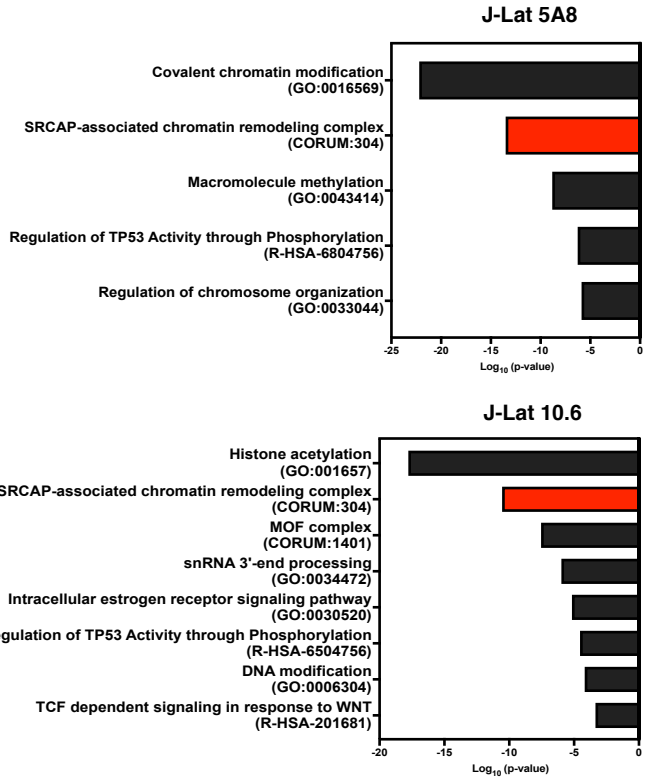

D

		-log$_{10}$ (MAGeCK Gene Score) J-Lat 5A8	J-Lat 10.6
NuA4 HAT complex	TRRAP	2.45	1.85
	EP400	2.38	2.24
	EPC2	0.99	1.33
	EPC1	0.38	0.47
	KAT5	6.43	3.83
	ING3	1.88	4.11
	MRGBP	0.88	0.26
	ACTB	0.19	0.75
	MORF4L1	1.30	2.61
	MORF4L2	1.34	1.18
	MEAF6	2.67	1.54
	MBTD1	1.96	1.17
SRCAP complex	BRD8	1.62	1.54
	DMAP1	4.46	7.22
	RUVBL2	1.25	1.76
	RUVBL1	1.96	0.32
	ACTL6A	7.32	13.10
	VPS72	4.24	6.98
	YEATS4	5.71	5.06
	SRCAP	4.51	4.20
	ACTR6	0.38	2.44
	ZNHIT1	4.11	2.13

Shared

Figure 4

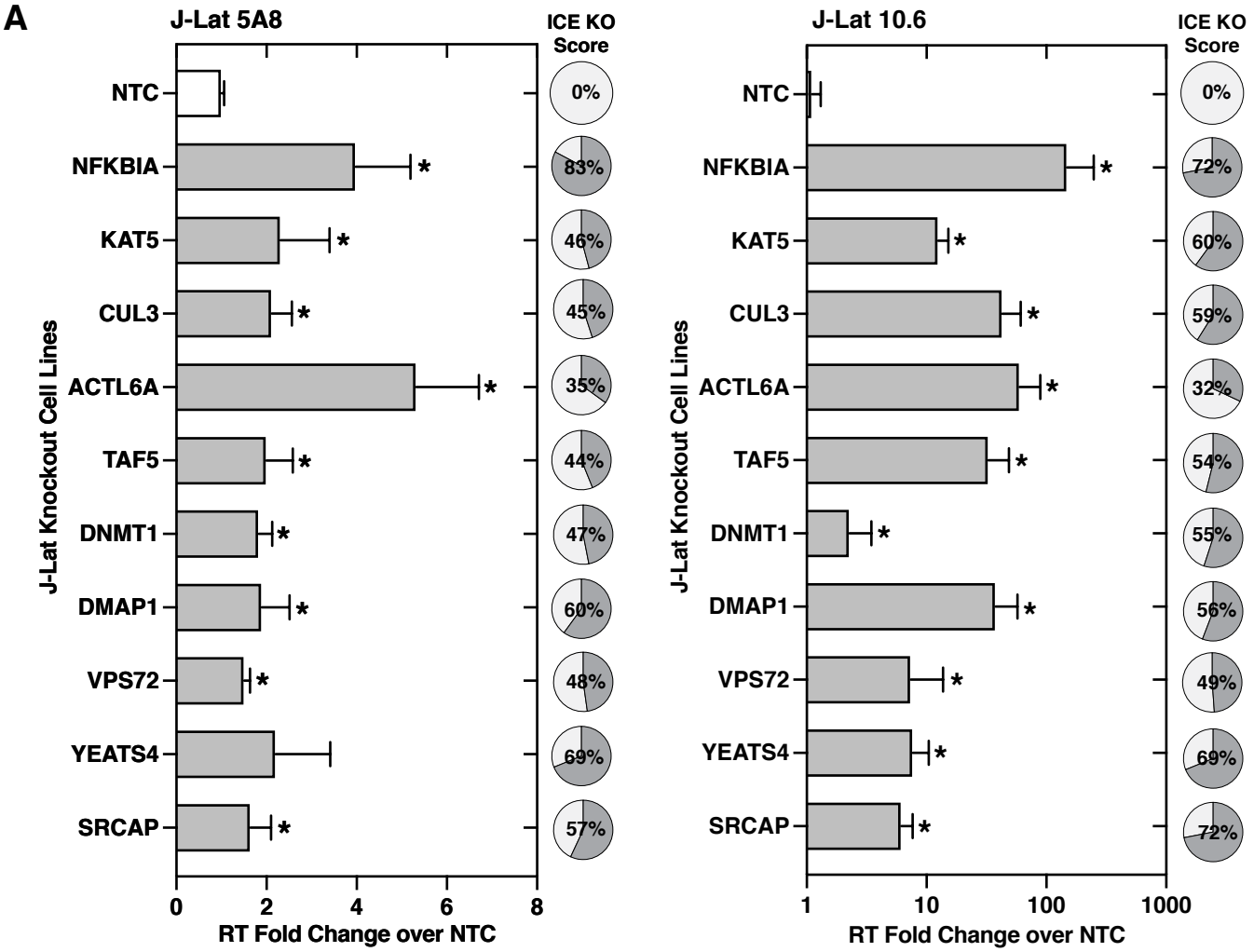
A
J-Lat 5A8
ICE KO Score
NTC
NFKBIA
KAT5
CUL3
ACTL6A
TAF5
DNMT1
DMAP1
VPS72
YEATS4
SRCAP
0%
83%
46%
45%
35%
44%
47%
60%
48%
69%
57%
J-Lat Knockout Cell Lines
0
2
4
6
8
RT Fold Change over NTC
J-Lat 10.6
ICE KO Score
0%
72%
60%
59%
32%
54%
55%
56%
49%
69%
72%
1
10
100
1000
RT Fold Change over NTC

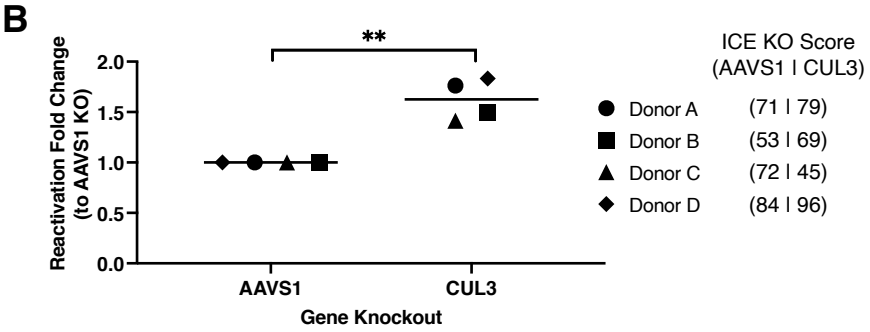
B
**
Reactivation Fold Change (to AAVS1 KO)
2.0
1.5
1.0
0.5
0.0
AAVS1
CUL3
Gene Knockout
ICE KO Score (AAVS1 I CUL3)
Donor A (71 I 79)
Donor B (53 I 69)
Donor C (72 I 45)
Donor D (84 I 96)

Figure 5

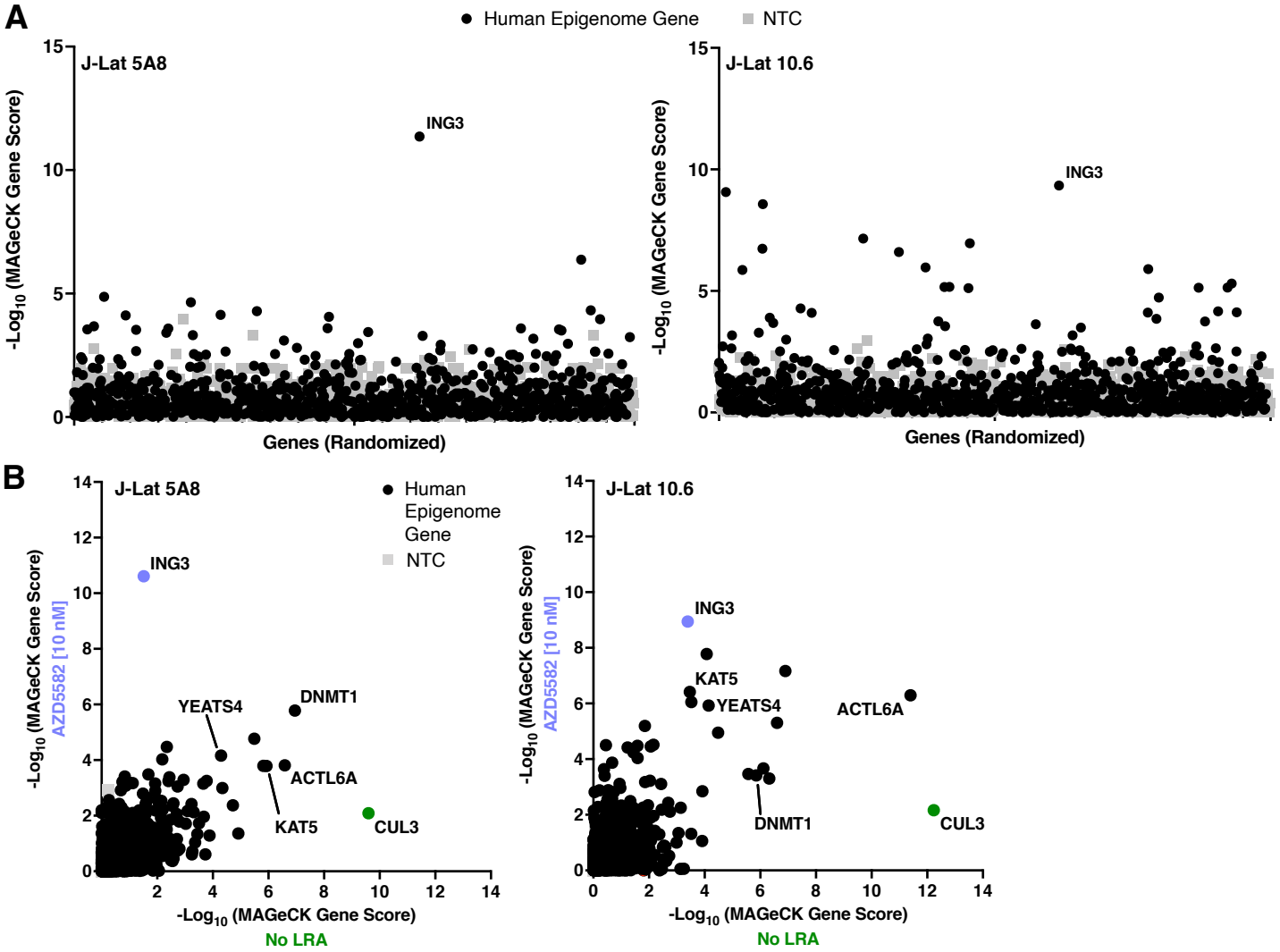
A
Human Epigenome Gene
NTC
J-Lat 5A8
ING3
-Log10 (MAGeCK Gene Score)
Genes (Randomized)
J-Lat 10.6
ING3
-Log10 (MAGeCK Gene Score)
Genes (Randomized)
B
J-Lat 5A8
Human Epigenome Gene
NTC
ING3
YEATS4
DNMT1
ACTL6A
KAT5
CUL3
-Log10 (MAGeCK Gene Score) AZD5582 [10 nM]
-Log10 (MAGeCK Gene Score) No LRA
J-Lat 10.6
ING3
KAT5
YEATS4
ACTL6A
DNMT1
CUL3
-Log10 (MAGeCK Gene Score) AZD5582 [10 nM]
-Log10 (MAGeCK Gene Score) No LRA

Figure 6

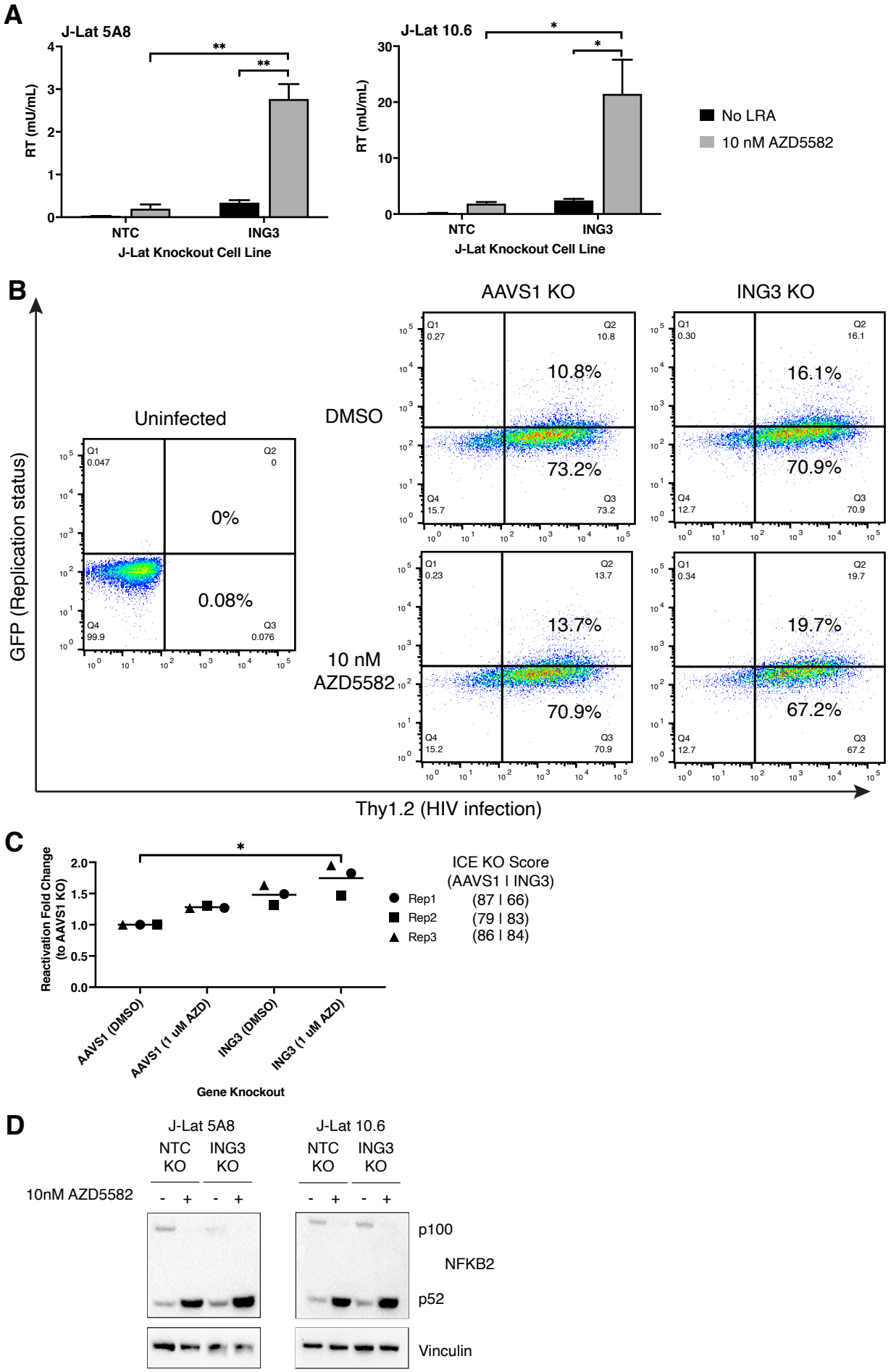
A
J-Lat 5A8
J-Lat 10.6
RT (mU/mL)
NTC
ING3
J-Lat Knockout Cell Line
No LRA
10 nM AZD5582
B
AAVS1 KO
ING3 KO
Uninfected
DMSO
10 nM AZD5582
0%
0.08%
10.8%
73.2%
16.1%
70.9%
13.7%
70.9%
19.7%
67.2%
GFP (Replication status)
Thy1.2 (HIV infection)
C
Reactivation Fold Change (to AAVS1 KO)
AAVS1 (DMSO)
AAVS1 (1 uM AZD)
ING3 (DMSO)
ING3 (1 uM AZD)
Gene Knockout
ICE KO Score (AAVS1 | ING3)
Rep1 (87 | 66)
Rep2 (79 | 83)
Rep3 (86 | 84)
D
J-Lat 5A8
J-Lat 10.6
NTC KO
ING3 KO
10nM AZD5582
p100
NFKB2
p52
Vinculin

Figure 7

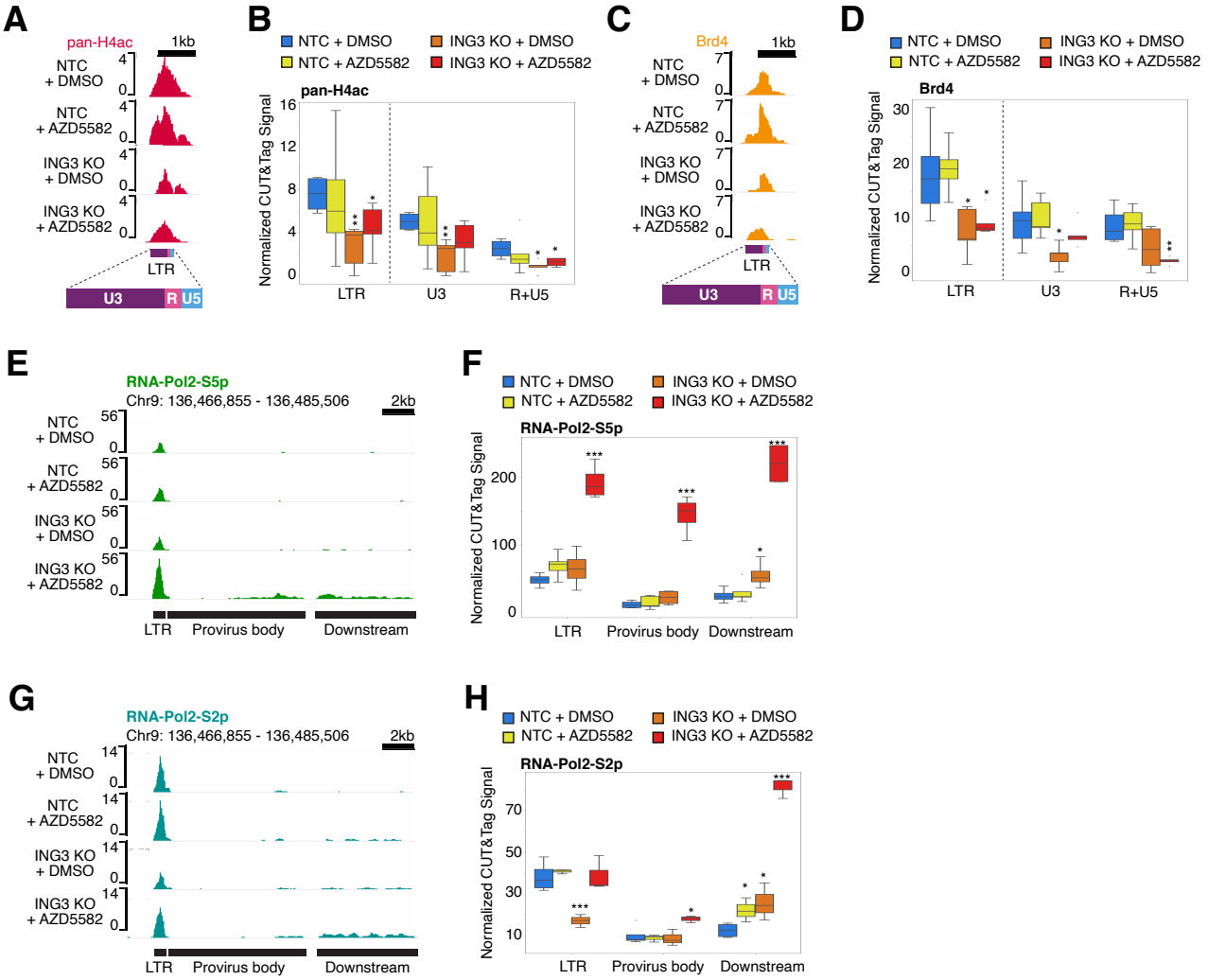
A
pan-H4ac
1kb
NTC + DMSO
NTC + AZD5582
ING3 KO + DMSO
ING3 KO + AZD5582
LTR
U3
R
U5
B
NTC + DMSO
NTC + AZD5582
ING3 KO + DMSO
ING3 KO + AZD5582
pan-H4ac
Normalized CUT&Tag Signal
LTR
U3
R+U5
C
Brd4
1kb
NTC + DMSO
NTC + AZD5582
ING3 KO + DMSO
ING3 KO + AZD5582
LTR
U3
R
U5
D
NTC + DMSO
NTC + AZD5582
ING3 KO + DMSO
ING3 KO + AZD5582
Brd4
Normalized CUT&Tag Signal
LTR
U3
R+U5
E
RNA-Pol2-S5p
Chr9: 136,466,855 - 136,485,506
2kb
NTC + DMSO
NTC + AZD5582
ING3 KO + DMSO
ING3 KO + AZD5582
LTR
Provirus body
Downstream
F
NTC + DMSO
NTC + AZD5582
ING3 KO + DMSO
ING3 KO + AZD5582
RNA-Pol2-S5p
Normalized CUT&Tag Signal
LTR
Provirus body
Downstream
G
RNA-Pol2-S2p
Chr9: 136,466,855 - 136,485,506
2kb
NTC + DMSO
NTC + AZD5582
ING3 KO + DMSO
ING3 KO + AZD5582
LTR
Provirus body
Downstream
H
NTC + DMSO
NTC + AZD5582
ING3 KO + DMSO
ING3 KO + AZD5582
RNA-Pol2-S2p
Normalized CUT&Tag Signal
LTR
Provirus body
Downstream

Figure 8

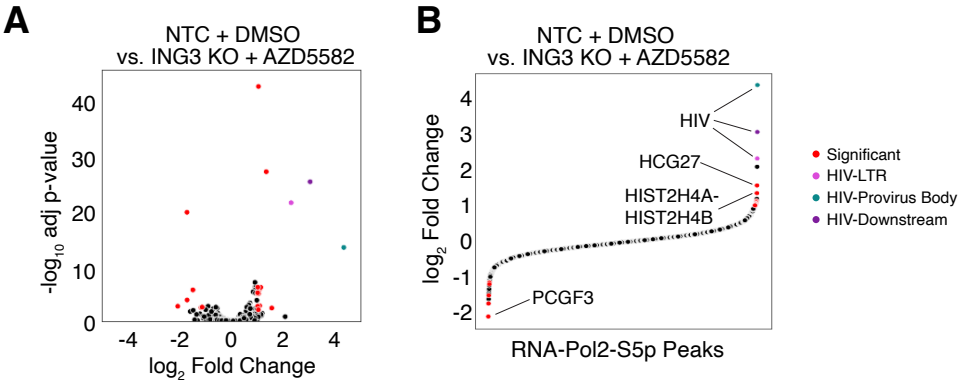
A
NTC + DMSO
vs. ING3 KO + AZD5582
-log10 adj p-value
log2 Fold Change
B
NTC + DMSO
vs. ING3 KO + AZD5582
log2 Fold Change
RNA-Pol2-S5p Peaks
HIV
HCG27
HIST2H4A-
HIST2H4B
PCGF3
Significant
HIV-LTR
HIV-Provirus Body
HIV-Downstream